

# A registration method for reduced basis problems using linear optimal transport\*

Tobias Blickhan<sup>1,2</sup>

<sup>1</sup> Max Planck Institute for Plasma Physics

<sup>2</sup> Technische Universität München

## Abstract

We present a registration method for model reduction of parametric partial differential equations with dominating advection effects and moving features. Registration refers to the use of a parameter-dependent mapping to make the set of solutions to these equations more amicable for approximation using classical reduced basis methods. The proposed approach utilizes concepts from optimal transport theory, as we utilize Monge embeddings to construct these mappings in a purely data-driven way. The method relies on one interpretable hyper-parameter. We discuss how our approach relates to existing works that combine model order reduction and optimal transport theory. Numerical results are provided to demonstrate the effect of the registration. This includes a model problem where the solution is itself a probability density and one where it is not.

## 1 Introduction

The field of reduced complexity modelling is of practical interest for numerous multi-query and real-time applications. Reduced methods can be constructed in an offline (or training) phase, leveraging the strengths of high-performance computing infrastructure. After construction reduced models can reduce the time, money, and energy spent on optimization loops, inverse problems, or routine calculations.

Classical methods such as the reduced basis approach [33, 28] provide ways to save orders of magnitude in computational cost while at the same time ensuring rigorous error bounds for the reduced simulation of elliptic and parabolic equations. However, they are notoriously ill-suited when working with hyperbolic systems or solutions with moving features and sharp discontinuities.

In this work, we present a registration method for model order reduction based on methods from optimal transport theory. The role of the registration step is to align the features in the solution data to make it more amicable for linear approximation. The method we propose is fully data-driven and therefore requires no previous knowledge of the form of the alignment mapping. Bijectivity of the mapping is connected to its construction from optimal transport theory and not enforced with penalty terms. One hyper-parameter set by the user controls the trade-off between accuracy and smoothness of the mapping. In an effort to keep the presentation self-contained, we recall some results from optimal transport theory and research that connects it to reduced complexity modeling.

## 2 Outline

The article is structured as follows: In section 3, we briefly review reduced basis and registration methods. Section 4 contains the concepts from optimal transport theory that will be used in our proposed method, which is described in section 5. Section 6 summarizes similar approaches from the literature and points out similarities and differences to our work. Two numerical examples are given in section 7. Specifics of computations related to optimal transport are presented in the supplementary material, appendix B.

---

\*Submitted to SIAM Journal on Scientific Computing

### 3 The reduced basis method

In this work, we will follow the classical reduced basis (RB) approach for parametrized partial differential equations (PPDEs) [33]. Given parameters  $\mu \in \mathcal{A}$ , we seek to solve many iterations of the following problem: Find a function  $u \in V_h$ , a discretized function space, such that

$$\mathcal{L}(u; \mu) = 0 \quad \text{in } \Omega, \quad (1)$$

together with suitable initial and boundary conditions which can again depend on  $\mu$ .

**Remark 1.** *In this work, we will treat the solution to the discretized problem as the true solution to the PPDE problem. Consequently, we omit the subscript  $_h$  from  $u$  to avoid notational clutter. Many of the following concepts are also well-defined if  $V_h$  is replaced by any Hilbert space.*

The set of all possible solutions to this problem is called the *solution manifold*

$$\mathcal{M} := \{u(\mu) \in V_h : \mathcal{L}(u(\mu); \mu) = 0 \text{ where } \mu \in \mathcal{A}\}. \quad (2)$$

If it is possible to approximate  $\mathcal{M}$  by a linear subspace of small dimension, the PPDE can be solved quickly and accurately for many values of  $\mu$  within this subspace. This property of  $\mathcal{M}$  is referred to as its *n-width* ([33], Section 5.4):

**Definition 1** (n-width). *The (Kolmogorov) n-width of  $\mathcal{M}$  is given by*

$$\inf_{\substack{V_n \subset V_h \\ \dim V_n = n}} \sup_{u \in \mathcal{M}} \inf_{u_{\text{rb}} \in V_n} \|u_{\text{rb}} - u\|_{V_h}. \quad (3)$$

An indicator of the n-width (a worst-case error measure) can be obtained by sampling  $\mathcal{M}$  and using an eigenvalue decomposition to estimate an average error. This method is known *proper orthogonal decomposition* (POD)

**Definition 2.** *The  $i$ th POD basis element of the set  $\{u(\mu_i)\}_{i=1}^{n_s}$  is given by*

$$\zeta_i = (\lambda_i^u)^{-\frac{1}{2}} \sum_{j=1}^{n_s} u(\mu_j) (v_i^u)_j, \quad (4)$$

where  $\lambda_i^u$  and  $v_i^u$  are the  $i$ th eigenvalue and eigenvector of the snapshot correlation matrix

$$\mathbb{C}^u := \{\langle u(\mu_i), u(\mu_j) \rangle_{V_h}\}_{1 \leq i, j \leq n_s}. \quad (5)$$

According to the Eckart–Young–Mirsky theorem, the space spanned by the POD basis of size  $n$  is optimal in the sense that  $\sum_{i=1}^n \|u(\mu_i) - \Pi_{\text{POD}} u(\mu_i)\|_{V_h}^2 = \sum_{i>n} \lambda_i$  is minimal, where  $\Pi_{\text{POD}}$  denotes the orthogonal projection onto  $\text{span}\{\zeta_i\}_{i=1}^n$ . Consequently, the decay of the eigenvalues of  $\mathbb{C}^u$  is a good indicator for how well a problem can be approximated using the classical RB method. While this decay can be shown to be exponential for, e.g., regular elliptic problems ([33], Section 5.5), this decay can be very slow for advection-dominated problems or problems with parameter-dependent geometry. This issue is well-known. One common strategy to overcome it is to find a suitable, parameter dependent mapping  $\Phi_\mu$  such that the manifold of mapped solutions

$$\Phi_\mu(\mathcal{M}) := \{u(\mu) \circ \Phi_\mu^{-1} : u(\mu) \in \mathcal{M}\} \quad (6)$$

has a much smaller n-width [38, 43, 27, 6, 51, 18]. This approach we refer to as *registration methods*. It leads to two challenges: First, a suitable mapping must be constructed (offline) and evaluated (online). Second, the mapped problem must be solved (online). The present work will focus on the first challenge, but we will also address how we tackle the second.

## 4 Optimal transport

Optimal transport (OT) theory provides a notion of distance between probability measures  $\rho, \sigma \in \mathcal{P}(\Omega_1) \times \mathcal{P}(\Omega_2)$ . In particular, a cost is modelled through a function  $c : \Omega_1 \times \Omega_2 \rightarrow \mathbb{R}$  where  $c(x, y)$  gives the cost of moving mass from  $x$  to  $y$ . In this work, we will look at the case where  $\Omega_1 = \Omega_2 = \Omega \subset \mathbb{R}^d$ . In all cases, we use the quadratic cost function  $c(x, y) = \frac{1}{2}|x - y|^2$ . The goal is to move mass that is distributed according to  $\rho$  to the configuration given by  $\sigma$ , while minimizing the total cost. Splitting mass is allowed, which leads to the following minimization problem:

**Definition 3** (OT distance). *The OT distance between  $\rho, \sigma \in \mathcal{P}(\Omega)$  with  $\Omega \subset \mathbb{R}^d$  compact is given by*

$$\text{OT}(\rho, \sigma)^2 := \inf_{\pi \in \Pi(\rho, \sigma)} \int_{\Omega \times \Omega} c(x, y) d\pi(x, y), \quad (7)$$

where  $\Pi(\rho, \sigma)$  is the set of admissible transport plans, i.e. probability measures on  $\Omega \times \Omega$  with fixed marginals:

$$\Pi(\rho, \sigma) := \{\pi \in \mathcal{P}(\Omega \times \Omega) : \pi(\cdot, \Omega) = \rho \text{ and } \pi(\Omega, \cdot) = \sigma\}. \quad (8)$$

The OT distance is also known as the *Wasserstein distance* or metric. A better name considering its history would be the *Kantorovich metric* [48].

A thorough introduction into the topic of optimal transport is beyond the scope of this work. We will repeat only a few select results for convenience. Proofs to the given propositions and theorems can be found in the excellent textbooks on the topic [31, 49, 39].

### 4.1 Transport potentials and c-transform

**Proposition 1** (OT duality). *The dual problem of eq. (7) is given by*

$$\text{OT}(\rho, \sigma)^2 = \sup_{\psi_\rho, \psi_\sigma \in \mathcal{C}_b(\Omega)} \left\{ \int_{\Omega} \psi_\rho d\rho + \int_{\Omega} \psi_\sigma d\sigma : \psi_\rho(x) + \psi_\sigma(y) \leq c(x, y) \right\}, \quad (9)$$

where  $\mathcal{C}_b$  denotes the space of bounded continuous functions. The duality gap is zero, so the two optimization problems are equivalent.

**Definition 4** (Transport potentials). *The functions  $\psi_\rho, \psi_\sigma \in \mathcal{C}_b(\Omega)$  from eq. (7) we call transport potentials. The name Kantorovich potentials can also be found in the literature to refer to those potentials solving the dual problem.*

Given that  $\rho$  and  $\sigma$  are probability measures, to maximise the objective in eq. (9), we want to make the potentials  $\psi_\rho, \psi_\sigma$  as large as possible without violating the constraint  $\psi_\rho \oplus \psi_\sigma \leq c$ . This leads to the notion of *c-transform*:

**Definition 5** (c-transform). *The c-transform of a function  $\psi : \Omega \rightarrow \mathbb{R} \cup \{+\infty\}$  is given by*

$$\psi^c(y) := \inf_{x \in \Omega} (c(x, y) - \psi(x)). \quad (10)$$

**Proposition 2.** *The potentials solving eq. (9) are c-conjugate to each other, i.e.  $\psi_\rho(x) = \psi_\sigma^c(x)$ .*

**Remark 2.** *In the case  $c(x, y) = \frac{1}{2}|x - y|^2$ , the c-transform is related to the Legendre transform by*

$$\frac{|y|^2}{2} - \psi^c(y) = \frac{|y|^2}{2} - \inf_{x \in \Omega} \left( \frac{1}{2}|x - y|^2 - \psi(x) \right) = \left( \frac{|x|^2}{2} - \psi(x) \right)^* =: \varphi^*(y). \quad (11)$$

If the measures are absolutely continuous with respect to the Lebesgue measure, there is no mass splitting, i.e. there exists a *transport map*  $T$  such that  $\sigma = T_{\#}\rho$ :

**Definition 6** (Push-forward). *The push-forward of  $\rho$  under  $T$ , denoted by  $T_{\#}\rho$ , is defined by  $(T_{\#}\rho)(\Omega') = \rho(T^{-1}(\Omega'))$  for all measurable  $\Omega' \subseteq \Omega$ . If both  $\rho$  and  $\sigma$  are absolutely continuous with densities denoted again  $\rho, \sigma$ , and  $T$  is a  $C^1$  diffeomorphism, then  $\sigma = T_{\#}\rho$  is equivalent to*

$$\rho = (\sigma \circ T) |\det DT|. \quad (12)$$

**Theorem 1** (Brenier’s theorem). *Assume  $\Omega \subset \mathbb{R}^d$  compact. If at least one of  $\rho, \sigma$  has a density with respect to the Lebesgue measure, then the unique solution to eq. (7) is concentrated on the graph  $(x, T(x))$  of the transport map  $T$ . In particular,*

$$\inf_{\pi \in \Pi(\rho, \sigma)} \frac{1}{2} \int_{\Omega \times \Omega} |x - y|^2 d\pi(x, y) = \inf_{T: \sigma = T\# \rho} \frac{1}{2} \int_{\Omega} |T(x) - x|^2 d\rho(x), \quad (13)$$

and  $T$  is the gradient of a convex function:

$$T(x) = \nabla \varphi = x - \nabla \psi(x). \quad (14)$$

The function  $\psi$  one of the two optimal transport potentials solving eq. (9), i.e.  $\psi_\rho$  corresponds to  $T_{\rho \rightarrow \sigma}$  and vice versa.

The map  $T$  is also called the *Monge map*.

**Remark 3.** *The push-forward density is also sometimes denoted  $\rho \circ T^{-1}$ . In this notation,  $\sigma = \rho \circ T_{\rho \rightarrow \sigma}^{-1} = \rho \circ (\text{id} - \nabla \psi_{\rho \rightarrow \sigma})^{-1} = \rho \circ (\text{id} - \nabla \psi_{\rho \rightarrow \sigma}^c) = \rho \circ (\text{id} - \nabla \psi_{\sigma \rightarrow \rho})$ . We denote by  $\psi_{\rho \rightarrow \sigma}$  the potential such that  $(\text{id} - \nabla \psi_{\rho \rightarrow \sigma})\# \rho = \sigma$ .*

## 4.2 Displacement interpolation and OT barycenters

Given the map  $T$ , one can visualize the optimal transport by introducing a time-like variable  $t$  to define  $T_t(x) := (1 - t)x + tT(x)$  and consider  $\rho_t := (T_t)\# \rho$ . The resulting path  $t \mapsto \rho_t$  through the space of probability measures is referred to as *displacement interpolation* [23] and illustrated in fig. 1.

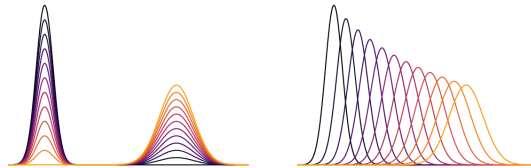


Figure 1:  $L^2$  interpolation and displacement interpolation between two Gaussian distributions.

The generalization to convex combinations of several distributions is called an *OT barycenter*:

**Definition 7** (OT barycenter). *Given a set of  $\{\rho_i\}_{i=1}^n \subset \mathcal{P}(\Omega)$  and non-negative, normalized weights  $\{\omega_i\}_{i=1}^n$ , the OT barycenter of  $\{\rho_i\}_{i=1}^n$  is given by*

$$\text{OTBar}(\{\omega_i, \rho_i\}_{i=1}^n) := \arg \min_{\sigma \in \mathcal{P}(\Omega)} \sum_{i=1}^n \omega_i \text{OT}(\rho_i, \sigma)^2. \quad (15)$$

When  $\omega_i \equiv n_s^{-1} \forall i$ , we omit the weights and write  $\text{OTBar}(\{\rho_i\}_{i=1}^n)$ .

## 4.3 Linear optimal transport

OT theory provides a metric on the space of probability measures with many favourable properties (e.g. the OT distance metrizes weak convergence for compact  $\Omega \subset \mathbb{R}^d$ ). Moreover, it allows us to (formally) treat  $\mathcal{P}(\Omega)$  as a Riemannian manifold, where the elements of the tangent space of  $\rho \in \mathcal{P}(\Omega)$  are elements of  $L^2(\rho, \mathbb{R}^d)$ . This allows a geometric and physical interpretation for the transport potentials  $\psi$ , which are the central objects of method. For more information on this geometric interpretation, we refer to [29] and [40, 1].

Given two distributions  $\rho$  and  $\sigma$ , the optimal transport map  $T_{\rho \rightarrow \sigma}$  from  $\rho$  to  $\sigma$  is an element of the tangent space  $L^2(\rho, \mathbb{R}^d)$ . Linear optimal transport (LOT) [50, 26, 24] works with these vector spaces. We recall the following definitions:

**Definition 8** (Monge embedding). *Given a fixed reference distribution  $\bar{\rho} \in \mathcal{P}(\Omega)$ , let  $T_{\bar{\rho} \rightarrow \sigma}$  denote the Monge map from  $\bar{\rho}$  to  $\sigma$ . The mapping  $\sigma \mapsto T_{\bar{\rho} \rightarrow \sigma}$  is called Monge embedding.*

**Definition 9** (LOT distance).

$$\text{LOT}^{\bar{\rho}}(\rho_1, \rho_2)^2 := \int_{\Omega} |T_{\bar{\rho} \rightarrow \rho_1} - T_{\bar{\rho} \rightarrow \rho_2}|^2 d\bar{\rho}. \quad (16)$$

**Definition 10** (LOT barycenter).

$$\text{LOTBar}^{\bar{\rho}}(\{\omega_i; \rho_i\}_{i=1}^n) := \arg \min_{\sigma \in \mathcal{P}(\Omega)} \sum_{i=1}^n \omega_i \text{LOT}^{\bar{\rho}}(\rho_i, \sigma)^2 = \left( \sum_{i=1}^n \omega_i T_{\bar{\rho} \rightarrow \rho_i} \right)_{\#} \bar{\rho}. \quad (17)$$

A natural question to ask is how well the LOT distance approximates the true OT distance. For general measures  $\rho, \sigma, \bar{\rho}$ , it holds that  $\text{OT}(\rho, \sigma) \leq \text{LOT}(\rho, \sigma) \leq \text{const.}(\Omega, d) \text{OT}(\rho, \sigma)^{\frac{2}{15}}$  ([26], Theorem 3.1), so the Monge embedding is not an isometry. With regularity assumptions on the measures, the exponent can be improved to  $\frac{1}{2}$  for measures along a Lipschitz curve through 2-Wasserstein space [16].

There are, however, special cases. For example, if  $\rho$  and  $\sigma$  are connected by shifts and scalings, i.e. a transformation of the form  $x \mapsto \bar{b}x + \bar{a}$  where  $0 < \bar{b} \in \mathbb{R}$  and  $\bar{a} \in \mathbb{R}^d$ , then  $\text{OT} = \text{LOT}$ . Furthermore, if the transformation connecting  $\rho$  to  $\sigma$  is  $\varepsilon$ -close to the form  $\bar{b}x + \bar{a}$ , then  $\text{LOT}(\rho, \sigma) \leq \text{OT}(\rho, \sigma) + C_1\varepsilon + C_2\sqrt{\varepsilon}$ . We refer to [24] for more details.

**Remark 4.** *The examples shown in section 7 are fundamentally scaling and translation mappings. In this context, OT and linear OT can be expected to perform well. For more complex transformations, and for transported measures that are not smooth densities (e.g.: curves), the fact that OT mappings do not preserve topology can become an issue. This difficulty is discussed in the context of shape analysis and medical imaging in [13] (see especially figures 3.31 and 3.32).*

#### 4.4 Entropic optimal transport

The classical OT problem can be modified by adding a regularizing term to the cost function eq. (7) as popularized by [8] (see [22] for a historical perspective going back to statistical physics considerations from the early 20th century). The resulting regularized problem can be solved numerically in a very efficient way (see appendix B).

**Definition 11** (Entropic OT). *Let  $\rho, \sigma, c, \Pi(\rho, \sigma)$  as in definition 3 and  $\varepsilon > 0$ . The OT problem with entropic regularization reads*

$$\begin{aligned} \text{OT}_{\varepsilon}(\rho, \sigma)^2 := & \min_{\pi \in \Pi(\rho, \sigma)} \int_{\Omega \times \Omega} c(x, y) d\pi^{\varepsilon}(x, y) + \varepsilon \int_{\Omega \times \Omega} \log \left( \frac{d\pi^{\varepsilon}(x, y)}{d\rho(x) d\sigma(y)} \right) d\pi^{\varepsilon}(x, y) \\ & - \varepsilon \int_{\Omega \times \Omega} d\pi^{\varepsilon}(x, y) + \varepsilon \int_{\Omega \times \Omega} d\rho(x) d\sigma(y). \end{aligned} \quad (18)$$

*The corresponding dual problem has the form*

$$\begin{aligned} \text{OT}_{\varepsilon}(\rho, \sigma)^2 = & \max_{\psi_{\rho}^{\varepsilon}, \psi_{\sigma}^{\varepsilon} \in \mathcal{C}_b(\Omega)} \int_{\Omega} \psi_{\rho}^{\varepsilon}(x) d\rho(x) + \int_{\Omega} \psi_{\sigma}^{\varepsilon}(y) d\sigma(y) \\ & - \varepsilon \int_{\Omega \times \Omega} \exp \left( \frac{\psi_{\rho}^{\varepsilon}(x) + \psi_{\sigma}^{\varepsilon}(y) - c(x, y)}{\varepsilon} \right) d\rho(x) d\sigma(y) + \varepsilon. \end{aligned} \quad (19)$$

Note that we recover the constraint  $\psi_{\rho} \oplus \psi_{\sigma} \leq c$  as  $\varepsilon \rightarrow 0$  in eq. (19). A formal computation shows that the stationarity conditions for this problem read

$$\exp \left( \frac{-\psi_{\sigma}^{\varepsilon}(y)}{\varepsilon} \right) = \int_{\Omega} \exp \left( \frac{\psi_{\rho}^{\varepsilon}(x) - c(x, y)}{\varepsilon} \right) d\rho(x) \quad \sigma - \text{a. e.} \quad \text{and} \quad (20)$$

$$\exp \left( \frac{-\psi_{\rho}^{\varepsilon}(x)}{\varepsilon} \right) = \int_{\Omega} \exp \left( \frac{\psi_{\sigma}^{\varepsilon}(y) - c(x, y)}{\varepsilon} \right) d\sigma(y) \quad \rho - \text{a. e.} \quad (21)$$

**Remark 5.** *At optimality, the double integral in eq. (19) evaluates to one due to eq. (20) and  $\text{OT}_{\varepsilon}(\rho, \sigma)^2$  is given by the sum of two weighted integrals of the potential functions.*

Taking the logarithm of eq. (20) defines the *softmin*, which replaces the *c-transform*:

**Definition 12** (softmin).

$$\begin{aligned}\psi^{c,\varepsilon}(y) &= -\varepsilon \log \int_{\Omega} \exp\left(\frac{\psi^{\varepsilon}(x) - c(x, y)}{\varepsilon}\right) d\rho(x) \\ &=: \min_{x \sim \rho}^{\varepsilon} \{c(x, y) - \psi^{\varepsilon}(x)\}\end{aligned}\tag{22}$$

**Remark 6.** *The fundamental difference to the classical OT problem is that for any  $\varepsilon > 0$ , the solution to eq. (18) necessarily has full support with respect to the product measure  $\rho \otimes \sigma$ . In contrast, it was concentrated on the graph of the Monge map for  $\varepsilon = 0$  in cases covered by theorem 1. The optimal solution lies in the interior of the set of admissible solutions and is characterized by optimality conditions of vanishing gradients [13].*

The parameter  $\varepsilon$  determines the strength of the regularization. As  $\varepsilon \rightarrow 0$ ,  $\min_{x \sim \rho}^{\varepsilon} \rightarrow \min_{x \in \text{supp } \rho}$  [13]. Furthermore, it holds that  $\|\nabla^k \psi\|_{\infty} = \mathcal{O}(1 + \varepsilon^{1-k})$  [14]. The properties of  $\text{OT}_{\varepsilon}$ , including its convergence as  $\varepsilon$  goes to zero has been studied extensively. We refer to [31, 13] for details. A useful practical interpretation is this: as the softmin operation is a Gaussian convolution, the entropic transport plan practically ignores features below the scale of  $\sqrt{\varepsilon}$ .

Just as in eq. (11), the case with no regularization, the potentials are linked to convex functions, defined through an approximate maximum:

**Proposition 3.** *The function*

$$\begin{aligned}y \mapsto \frac{1}{2}|y|^2 - \psi^{c,\varepsilon}(y) &= \varepsilon \log \int_{\Omega} \exp\left(\frac{1}{\varepsilon}\left(x \cdot y - \frac{1}{2}|x|^2 + \psi^{\varepsilon}(x)\right)\right) d\rho(x) \\ &=: \max_{x \sim \rho}^{\varepsilon} \left\{x \cdot y - \left(\frac{1}{2}|x|^2 - \psi^{\varepsilon}(x)\right)\right\}\end{aligned}\tag{23}$$

*is convex.*

*Proof.* Evaluate the function at  $y_t := ty_1 + (1-t)y_2 : 0 < t < 1$  and apply Hölder's inequality with exponents  $\frac{1}{t}, \frac{1}{1-t}$ .  $\square$

**Remark 7.** *The particular value of  $\varepsilon$  plays no role for convexity. The limit cases  $\varepsilon \rightarrow 0 : \max_{x \sim u}^{\varepsilon} \rightarrow \max_{x \in \text{support } \rho}$  and  $\varepsilon \rightarrow \infty : \max_{x \sim \rho}^{\varepsilon} \rightarrow \int_{\Omega} d\rho$  are also convex.*

In practice, the  $\text{OT}_{\varepsilon}$  dual problem is solved by iteratively applying the softmin operation until the potentials fulfill eq. (20) and  $\psi_{\rho}^{\varepsilon} = \psi_{\sigma}^{c,\varepsilon}$ . The solution to the primal problem is then given by  $\pi^{\varepsilon} = \rho \otimes \sigma \exp\left(\frac{1}{\varepsilon}(\psi_{\rho}^{\varepsilon} \oplus \psi_{\sigma}^{\varepsilon} - c)\right)$ .

**Remark 8.** *The number of iterations needed to solve the entropic OT problem in practice go up dramatically as  $\varepsilon \rightarrow 0$ . In particular, in simple cases where the solution for  $\varepsilon = 0$  is a smooth map, the error after the  $l$ th iteration is of order  $(1 - \varepsilon)^l$  ([31], Remark 4.15). For the moderately small values of  $\varepsilon$  (when compared to the characteristic scale of the cost function) used in this work, this is not yet very restrictive. Beyond that, however, simulated annealing and multi-scale methods become necessary (c.f. [13], Section 3.3.3 and [31], Section 4.2).*

The entropic OT problem does not admit a transport map as a solution, as the transport plan is necessarily supported on the entirety of  $\rho \otimes \sigma$ . It is a natural question what the map  $x \mapsto x - \nabla \psi_{\rho}^{\varepsilon}(x)$  corresponds to. From the stationarity condition eq. (20), we find

$$\begin{aligned}\nabla \psi_{\rho}^{\varepsilon}(x) &= \frac{\int_{\Omega} (x - y) \exp\left(\frac{1}{\varepsilon}(\psi_{\sigma}^{\varepsilon}(y) - c(x, y))\right) d\sigma(y)}{\int_{\Omega} \exp\left(\frac{1}{\varepsilon}(\psi_{\sigma}^{\varepsilon}(y) - c(x, y))\right) d\sigma(y)} \\ &= x - \frac{\int_{\Omega} y \exp\left(\frac{1}{\varepsilon}(\psi_{\sigma}^{\varepsilon}(y) - c(x, y))\right) d\sigma(y)}{\int_{\Omega} \exp\left(\frac{1}{\varepsilon}(\psi_{\sigma}^{\varepsilon}(y) - c(x, y))\right) d\sigma(y)} \\ &=: x - T_{\rho \rightarrow \sigma}^{\varepsilon}(x)\end{aligned}\tag{24}$$

**Definition 13** (Entropic Monge map). We call  $T_{\rho \rightarrow \sigma}^\varepsilon = \text{id} - \nabla \psi_\rho^\varepsilon$  the entropic Monge map between  $\rho$  and  $\sigma$ .

It must be stressed that  $T_\#^\varepsilon \rho \neq \sigma$  in general. Nevertheless, the map has appealing properties: It is defined for all  $y \in \Omega$  (not only  $\rho$  - almost everywhere) and converges to the Monge map in  $L^2(\rho)$  as  $\varepsilon \rightarrow 0$  [32]. The entropic Monge map can also be interpreted as an extension of the expected value  $x \mapsto \mathbb{E}_{\pi^\varepsilon}[Y|X=x]$  from  $\text{support}(\rho)$  to the entire domain. It is also referred to as the *barycentric mapping* [13] as it has the form of a weighted mean with normalized weights.

## 4.5 Sinkhorn divergences

While the OT problem without regularization defines a distance on  $\mathcal{P}$ , this does not hold for the entropic version  $\text{OT}_\varepsilon$ . In general,  $\text{OT}_\varepsilon(\rho, \rho) \neq 0$  and there exist measures  $\sigma$  such that  $\text{OT}_\varepsilon(\rho, \sigma) < \text{OT}_\varepsilon(\rho, \rho)$  [13]. Indeed, as stated in [20], Proposition 1, we have

$$\text{OT}_\varepsilon(\rho, \rho)^2 = \max_{\psi \in \mathcal{C}_b(\Omega)} \left( 2 \int_\Omega \psi \, d\rho - \varepsilon \int_{\Omega \times \Omega} \exp\left(\frac{\psi \oplus \psi - c}{\varepsilon}\right) \, d\rho \, d\rho + \varepsilon \right) = 2 \int_\Omega \psi_{\rho \rightarrow \rho}^\varepsilon \, d\rho \quad (25)$$

where  $\psi_{\rho \rightarrow \rho}^\varepsilon$  solves  $e^{-\frac{\psi_{\rho \rightarrow \rho}^\varepsilon(x)}{\varepsilon}} = \int_\Omega e^{\frac{\psi_{\rho \rightarrow \rho}^\varepsilon(y) - c(x,y)}{\varepsilon}} \, d\rho(y) \, \rho - a.e..$

**Remark 9.** Consequently, fitting problems of the form  $\min_\sigma \text{OT}_\varepsilon(\rho, \sigma)$  usually do not converge to  $\rho$ .

As discussed in [34, 15], the *Sinkhorn divergence*

$$S_\varepsilon(\rho, \sigma)^2 := \text{OT}_\varepsilon(\rho, \sigma)^2 - \frac{1}{2} \text{OT}_\varepsilon(\rho, \rho)^2 - \frac{1}{2} \text{OT}_\varepsilon(\sigma, \sigma)^2 \quad (26)$$

remedies this issue and defines a distance for any value of  $\varepsilon$ . As shown in [34, 15],  $S_\varepsilon(\rho, \sigma)$  converges to  $\text{OT}(\rho, \sigma)$  as  $\varepsilon$  goes to zero under mild assumptions on the densities. For  $\varepsilon \rightarrow +\infty$ ,  $S_\varepsilon$  approaches a *maximum mean discrepancy* distance with the cost function as its kernel. We refer to [13], Section 3.2.3 for details.

The solution to eq. (26) involves four potentials, two for the transport between  $\rho$  and  $\sigma$  stemming from the  $\text{OT}_\varepsilon(\rho, \sigma)$  term which we will denote  $\psi_{\rho \rightarrow \sigma}, \psi_{\sigma \rightarrow \rho}$  and two potentials  $\psi_{\sigma \rightarrow \sigma}, \psi_{\rho \rightarrow \rho}$  from the added terms:

$$S_\varepsilon(\rho, \sigma)^2 = \int_\Omega (\psi_{\rho \rightarrow \sigma}^\varepsilon - \psi_{\rho \rightarrow \rho}^\varepsilon) \, d\rho + \int_\Omega (\psi_{\sigma \rightarrow \rho}^\varepsilon - \psi_{\sigma \rightarrow \sigma}^\varepsilon) \, d\sigma. \quad (27)$$

We can define the entropic Monge map analogously as

$$T_{\rho \rightarrow \sigma}^{\varepsilon, \text{debiased}} := \text{id} - \nabla \psi_{\rho \rightarrow \sigma} + \nabla \psi_{\rho \rightarrow \rho}. \quad (28)$$

## 4.6 Entropic bias

Let  $\pi, \varsigma \in \mathcal{P}(\Omega \times \Omega)$  and

$$\text{KL}(\pi|\varsigma) := \int_{\Omega \times \Omega} \left( \log \left( \frac{d\pi}{d\varsigma} \right) \, d\pi - d\pi + d\varsigma \right). \quad (29)$$

We observe that  $\text{OT}_\varepsilon(\rho, \sigma)^2 = \min_{\pi^\varepsilon \in \Pi(\rho, \sigma)} (\int_{\Omega \times \Omega} c(x, y) \, d\pi^\varepsilon(x, y) + \varepsilon \text{KL}(\pi^\varepsilon | \rho \otimes \sigma))$  and  $\text{KL}(\pi|\varsigma_1) = \text{KL}(\pi|\varsigma_2) + \text{KL}(\varsigma_2|\varsigma_1) \, \forall \varsigma_1, \varsigma_2 \in \mathcal{P}(\Omega \times \Omega)$ .

Let  $\text{OT}_\varepsilon^\varsigma(\rho, \sigma)^2 := \min_{\pi^\varepsilon \in \Pi(\rho, \sigma)} (\int_{\Omega \times \Omega} c(x, y) \, d\pi^\varepsilon(x, y) + \varepsilon \text{KL}(\pi^\varepsilon | \varsigma))$ . The choice  $\varsigma = \rho \otimes \sigma$  in the definition of  $\text{OT}_\varepsilon$  (no superscript) is natural, as  $\pi^\varepsilon$  is guaranteed to be absolutely continuous with respect to this product measure. However, many other choices (e.g. one that is constant on  $\text{supp}(\rho \otimes \sigma)$ ) are also possible. Choosing two different  $\varsigma_1, \varsigma_2$  changes the value of  $\text{OT}_\varepsilon^{\varsigma_1}$  by the constant  $\text{KL}(\varsigma_2|\varsigma_1)$ .

When computing OT barycenters, a different choice of  $\varsigma$  leads to

$$\text{OTBar}_\varepsilon^\varsigma(\{\omega_i; \rho_i\}_{i=1}^n) = \arg \min_{\sigma \in \mathcal{P}(\Omega)} \sum_{k=1}^n \omega_k \{ \text{OT}_\varepsilon(\rho_k, \sigma)^2 + \varepsilon \text{KL}(\varsigma | \rho_k \otimes \sigma) \}. \quad (30)$$

Selecting the Lebesgue measure as  $\varsigma$  leads to entropic smoothing, blurring the barycenter. This effect is discussed in [9, 42]. In [20], it is shown that when all input measures are Gaussian  $\rho_k = \mathcal{N}(\mu_k, \text{var})$ , the entropic barycenter using the Lebesgue measure in KL will be a Gaussian  $\mathcal{N}(\sum_k \omega_k \mu_k, \text{var} + \varepsilon)$ . The choice of the product measure leads to  $\mathcal{N}(\sum_k \omega_k \mu_k, \text{var} - \varepsilon)$  for  $\text{var} > \varepsilon$  and  $\delta_{\sum_k \omega_k \mu_k}$  otherwise.

This smoothing (resp. shrinking) bias can be seen as a feature of the method, as in [36] it is shown that the entropic shrinking corresponds to a maximum-likelihood deconvolution technique. Alternatively, one can remove the effect of the choice in KL by replacing  $\text{OT}_\varepsilon$  with  $S_\varepsilon$ : It is straightforward to show that the value of  $S_\varepsilon$  no longer depends on  $\varsigma$ , but only on  $\text{KL}(\pi_{\rho, \sigma}^\varepsilon | \pi_{\rho, \rho}^\varepsilon)$  and  $\text{KL}(\pi_{\rho, \sigma}^\varepsilon | \pi_{\sigma, \sigma}^\varepsilon)$ . For the example of Gaussians  $\rho_k = \mathcal{N}(\mu_k, \text{var})$ , the  $S_\varepsilon$  barycenter is a  $\mathcal{N}(\sum_k \omega_k \mu_k, \text{var}) \forall 0 < \varepsilon < +\infty$  ([20], Theorem 3).

In the following, replacing  $\text{OT}_\varepsilon$  by  $S_\varepsilon$  will be referred to as *de-biased* OT and de-biased barycenter will be used to refer to  $\arg \min_{\sigma \in \mathcal{P}(\Omega)} \sum_{k=1}^n \omega_k S_\varepsilon(\rho_k, \sigma)^2$ .

## 5 Transport mappings for reduced bases

**Remark 10.** *In this section, all quantities related to OT ( $\psi, \psi^c, T, \dots$ ) are denoted by their un-regularized form. The proposed method is applicable in this setting under sufficient regularity assumptions discussed in section 5.5. For computational feasibility, we use entropic regularization in practice. To apply the method in this case, one has to make the appropriate replacements, i.e. the  $c$ -transform becomes an application of the softmin, OT becomes  $\text{OT}_\varepsilon$  or  $S_\varepsilon$ ,  $\psi_{\rho \rightarrow \sigma}$  becomes either  $\psi_{\rho \rightarrow \sigma}^\varepsilon$  or  $\psi_{\rho \rightarrow \sigma}^\varepsilon - \psi_{\rho \rightarrow \rho}^\varepsilon$ , and so forth. When specific assumptions or steps change depending on what regularisation is used, it is explicitly stated.*

As a motivating example, consider the pure advection equation.

**Example 1.** *The PPDE  $\partial_t \rho + \bar{a} \partial_x \rho = 0$  with initial condition  $\rho_0 = \mathbb{1}_{(-1, 0]}$ , a fixed advection  $\bar{a} > 0$ , and parameter  $t \in \mathcal{A} = [0, T]$  on the domain  $\Omega = [-1, 1]$  is a prototypical example of a problem with very slow  $n$ -width decay of the solution manifold  $\mathcal{M} = \{x \mapsto \rho_0(x - \bar{a}t) : t \in [0, 1]\}$ . The  $n$ -width in this case decays as slow as  $\sim n^{1/2}$  [12].*

In contrast, if we set  $\bar{\rho} = \rho_0$ , the Monge embeddings of the set of solutions are of the form  $\{T_{\bar{\rho} \rightarrow \rho(t)}(y) = y + \bar{a}t : t \in [0, 1]\}$  with the corresponding potentials  $\{\psi_t^c(y) = -\bar{a}ty : t \in [0, 1]\}$ . Clearly, this is a one-dimensional linear space.

### 5.1 Dimension reduction on the Monge embeddings

Consider a PPDE problem with solution  $u(\mu)$  and related densities  $\rho(u)(\mu) =: \rho(\mu)$ . In some cases,  $\rho(u) = u$  is a possible choice, as in example 1. The requirements for  $\rho$  are that it returns probability densities that coincide with the features of the solution that have to be registered. In [19], a scalar testing function  $\mathcal{T}$  is chosen to determine the distribution of features (which are sets of points  $\{x \in \Omega : \mathcal{T}(x; u) > 0\}$ ). Examples for  $\mathcal{T}$  considered therein include  $\|\nabla \times u\|$ ,  $\|\nabla u\|$ , the derivative of the Mach number of a flow, and a shock discontinuity indicator (equation (34) therein). For the proposed method,  $\rho$  should return continuous densities supported on the entire domain, see section 5.5. In the numerical examples, we use  $\rho(u) = \frac{|u(\mu)|^2}{\int |u(\mu)|^2}$  as one example.

The discretization of  $u$  and  $\rho$  also need not agree. It can be beneficial to discretise the latter on a regular tensor grid, see appendix B.

Given a set of snapshots  $\{u(\mu_i)\}_{i=1}^{n_s} \subset V_h$ , compute  $\{\rho(u)(\mu_i)\}_{i=1}^{n_s}$  and denote by  $\bar{\rho}$  a suited reference density, e.g.  $\rho(\bar{\mu})$  for a certain parameter value  $\bar{\mu}$ , or a weighted OT barycenter of  $\{\rho(\mu_i)\}_{i=1}^{n_s}$ . Next, calculate the Monge embeddings  $\{T_{\bar{\rho} \rightarrow \rho(\mu_i)}\}_{i=1}^{n_s}$ . We denote by  $\psi_i^c$  the transport potential such that  $T_{\bar{\rho} \rightarrow \rho(\mu_i)}(y) = y - \nabla \psi_i^c(y)$ .

**Definition 14.** *The transport modes of a set of probability measures  $\{\rho(\mu_i)\}_{i=1}^{n_s}$  and a reference  $\bar{\rho}$  are given by  $y \mapsto \xi_j^c(y) = (\lambda_j^\psi)^{-1/2} \sum_{i=1}^{n_s} (v_j^\psi)_i \psi_i^c(y)$ , where  $\lambda_j^\psi$  and  $v_j^\psi$  are  $j$ th non-zero eigenvalue and eigenvector of the Monge embedding correlation matrix*

$$\mathbb{C}^\psi := \{ \langle \nabla \psi_i^c, \nabla \psi_j^c \rangle_{L^2(\bar{\rho})} \}_{1 \leq i, j \leq n_s}. \quad (31)$$



Note the similarities with definition 2 for the POD modes.

**Example 2.** For snapshots of the pure advection equation at different times  $t_i \in [0, T]$ :  $\{\rho_0(x - \bar{a}t_i)\}_{i=1}^{n_s}$ , we find  $(\mathbb{C}^\psi)_{ij} = \bar{a}^2 t_i t_j$  with one non-zero eigenvalue  $\lambda_1^\psi = \bar{a}^2 \sum_{i=1}^{n_s} t_i^2$  and eigenvector  $(v_1^\psi)_i = t_i (\sum_{j=1}^{n_s} t_j^2)^{-1/2}$ . The corresponding transport mode is given by  $\xi_1^c(y) = -y$ .

If the eigenvalues of  $\mathbb{C}^\psi$  decay fast enough, all transport potentials  $\psi^c(\mu)$  can be accurately (in the sense of a  $\bar{\rho}$ -weighted  $L^2$  norm of their derivatives) approximated by a linear combination of the form  $\psi^c(\mu) \approx \sum_{j=1}^m w_j(\mu) \xi_j^c$  where  $m \ll n_s$ .

**Remark 11.** We assume here that the map  $\mu \rightarrow \psi^c(\mu)$  is very regular. This can be the case even if the mapping  $\mu \mapsto u(\mu)$  is not (which can cause problems for reduced order modelling in the first place, see [33], Section 5.3) and even if  $\rho(u) = u$ . Consider for example  $\mathcal{M} = \{u(\mu) = \mathcal{N}(\mu, \text{var}) : \mu \in \mathbb{R}\}$ . The map  $\mu \mapsto u(\mu) \in L^1$  has a Lipschitz constant of  $\frac{1}{\text{var}}$ , while the map  $\mu \mapsto T_\mu = \text{id} - \mu + \bar{\mu}$  is 1-Lipschitz for  $\bar{\rho} = \rho(u)(\bar{\mu})$ .

## 5.2 Reference reduced basis

Evaluating

$$u(\mu_i) \circ \left( \text{id} - \nabla \sum_{j=1}^m w_j(\mu) \xi_j^c \right) =: u(\mu_i) \circ \Phi_\mu^{-1} \quad (32)$$

applies the approximated transport mapping to the  $i$ th snapshot and yields elements of the mapped snapshot manifold  $\Phi_\mu(\mathcal{M})$ . By construction, we expect this set to be more amicable to linear approximation. Returning to the simplest example, In the pure advection case, there is only one transport mode of the form  $\xi_1^c(y) = -y$ . The approximation of the snapshot potentials  $\psi_i^c = -\bar{a}t_i y \in \text{span}\{\xi_1^c\} \forall i$  is exact and the mapped snapshot manifold consists of one single element.

More generally, we proceed by building a reduced basis in the reference space using the correlation matrix of transported snapshots

$$\mathbb{C}^{\Phi^*u} := \{\langle u(\mu_i) \circ \Phi_{\mu_i}^{-1}, u(\mu_j) \circ \Phi_{\mu_j}^{-1} \rangle_{V_h}\}_{1 \leq i, j \leq n_s}. \quad (33)$$

Just as in the classical RB method described in section 3, we obtain a set of reduced basis functions which we will denote by  $\phi_1, \dots, \phi_{n_m}$ . Now, any element of  $\mathcal{M}$  can be approximated via

$$u_{\text{trb}}(\mu) := \sum_{i=1}^{n_m} \tilde{u}(\mu)_i \phi_i \circ \left( \text{id} - \nabla \left[ \sum_{j=1}^m w_j(\mu) \xi_j^c \right]^c \right) = \sum_{i=1}^{n_m} \tilde{u}(\mu)_i \phi_i \circ \Phi_\mu. \quad (34)$$

**Remark 12.** We use the properties of the  $c$ -transform to invert the mapping. This trick is possible since the gradients of Legendre transforms are inverses of each other ([17], Remark 0.1) and the  $c$ -transform and Legendre transform are related through eq. (11), as long as  $\sum_{j=1}^m w_j(\mu) \xi_j^c$  is in fact a transport potential, i.e. a convex function (see section 5.4).

We conclude this subsection with an example for a one-dimensional PPDE that forms boundary layers from [43]:

**Proposition 4.** The solutions to the equation

$$-\partial_{xx}^2 u_\mu + \mu^2 u_\mu = 0 \quad (35)$$

on the domain  $\Omega = (0, 1)$  with boundary conditions  $u_\mu(0) = 1$ ,  $u_\mu(1) = 0$  and  $\mu, \bar{\mu} \in [\mu_{\min}, \mu_{\max}] =: \mathcal{A}$ ,  $\mu_{\max} = \epsilon^{-2} \mu_{\min}$ ,  $\mu_{\min} > 1$ ,  $\epsilon \in (0, 1)$  satisfy

$$\inf_{\xi_1^c \in \text{span}\{\psi_{\bar{\mu}}^c : \mu \in \mathcal{A}\}} \sup_{\mu \in \mathcal{A}} \inf_{\substack{w_1(\mu) \in \mathbb{R} \\ \Phi_\mu^{-1}(y) = y - w_1(\mu) \partial_y \xi_1^c(y) \\ \Phi_\mu^{-1} : \Omega \rightarrow \Omega \text{ is a bijection}}} \|u_{\bar{\mu}} - u_\mu \circ \Phi_\mu^{-1}\|_{L^2(\Omega)} \leq e^{-\mu_{\min}} (4 + \epsilon). \quad (36)$$

where  $\rho(u) = \frac{u}{\int u}$ ,  $\bar{\rho} = \text{OTBar}(\{\rho_\mu : \mu \in \mathcal{A}\})$ , and  $\psi_\mu^c$  denotes the function such that  $T_{\bar{\rho} \rightarrow \rho_\mu}(y) = y - \partial_y \psi_\mu^c(y)$  and  $\int \psi_\mu^c = 0$ .

In other words, we can show a bound on the Kolmogorov n-m-width (in the limit of tolerance  $\rightarrow 0$ , c.f. [43], section 3.2) of  $\mathcal{M}$  for  $n = m = 1$ . The proof of this proposition can be found in appendix D.

### 5.3 Online phase

To solve the PPDE problem for a new parameter value  $\mu$ , we determine the mapping  $\Phi_\mu$ , which is determined by the values of  $w_{1,\dots,m}(\mu)$ . Next, we plug the expression (34) into the discretized PDE, and solve for  $\tilde{u}_{1,\dots,n_m}(\mu)$ . In this work, we learn the mapping  $\mu \mapsto w_{1,\dots,m}(\mu)$  using a Gaussian process [35] and the data from the snapshot set  $\{\mu_i, w_{1,\dots,m}(\mu_i)\}_{i=1}^{n_s}$ . The functions could also be described by interpolation or any related method. We use the Gaussian process as it is computationally cheap also for high-dimensional data.

The system of equations for  $\tilde{u}_{1,\dots,n_m}(\mu)$  is then obtained by Galerkin projection using the reference reduced basis  $\phi_{1,\dots,n_m}$ . For example, a bilinear form corresponding to a Laplace operator reads

$$\int_{\Omega} \nabla(\phi_j \circ \Phi_\mu) \cdot \nabla(\phi_j \circ \Phi_\mu) dx = \int_{\Phi_\mu(\Omega)} \nabla \phi_j \cdot [D\Phi_\mu^{-1}]^{-1} [D\Phi_\mu^{-1}]^{-T} \nabla \phi_j | \det D\Phi_\mu^{-1} | dy \quad (37)$$

where  $\Phi_\mu(\Omega) = \Omega$  and  $D\Phi_\mu^{-1} = \text{Id} - \sum_{j=1}^m w_j(\mu) D^2 \xi_j^c$ .

**Remark 13.** *The drawback is that these forms have to be assembled for every new parameter value, and the computational cost for this depends on the dimension of the full-order problem. This is a challenge to any projection-based model order reduction method that utilizes a parameter-dependent mapping and requires hyper-reduction techniques to solve, see section 5.6.*

**Remark 14.** *If the parameters are time-dependent, or time is itself a parameter, the online phase will also feature an additional advection-like term:*

$$\frac{d}{dt} u_{\text{trb}}(\mu) = \sum_{i=1}^{n_m} \left( \frac{d\tilde{u}(\mu)_i}{dt} \phi_i \circ \Phi_\mu + \tilde{u}(\mu)_i \frac{d\Phi_\mu}{dt} \cdot (\nabla \phi_i \circ \Phi_\mu) \right) \quad (38)$$

*In the reference domain, this requires the evaluation of  $\frac{d\Phi_\mu}{dt} \circ \Phi_\mu^{-1} = -[D\Phi_\mu^{-1}]^{-T} \frac{d\Phi_\mu^{-1}}{dt}$ . Evaluating the latter expression is done using  $\frac{d\Phi_\mu^{-1}}{dt} = -\sum_{j=1}^m \frac{dw_j(\mu)}{dt} \nabla \xi_j^c$ .*

In summary, our proposed approach relies on snapshot remapping. The difference to other existing methods of this form is how the mappings are obtained. Our approach is data-driven and based on a POD of Monge embeddings. Other choices for parameter dependent mappings in the literature include problem-dependent parametrizations [6], polynomial expansion [27, 51], and high-fidelity piece-wise polynomial mappings [43] (see also section 6 for a comparison of this approach and our method).

### 5.4 Invertibility and boundary conditions of the mapping

For now, assume  $\Omega = [0, 1]^{d \in \{2,3\}}$ , the unit square or cube. Proposition 2.3 in [43] proves two sufficient conditions in order for a mapping of the form  $\Phi^{-1}(y) = y - \sum_{j=1}^m w_j \nabla \xi_j^c$  to be a bijection in this case: Firstly,  $\nabla \xi_j^c \cdot \hat{e}_i = 0 : 1 \leq i \leq d$  on all edges (faces), where  $\hat{e}_{1,\dots,d}$  are normal vectors, and secondly  $\det D\Phi^{-1} > 0$  in  $\Omega \cup \partial\Omega$ . In the case of more general mappings from  $\Omega_2$  to  $\Omega_1$ , the first condition reads  $\text{dist}(\Phi^{-1}(y), \partial\Omega_1) = 0 \forall y \in \partial\Omega_2$  (Proposition 2.4 therein).

A natural question is if these conditions are met by the mappings defined in this section. We can give some answers in the non-regularized case. Suppose that  $\psi^c$  is the Kantorovich potential for the transport from  $\bar{\rho} \in \mathcal{P}(\Omega_2)$  to  $\rho \in \mathcal{P}(\Omega_1)$ , and both  $\bar{\rho}$  and  $\rho$  admit densities. Then, from theorem 1, we know that the transport map is given by  $\nabla \varphi^* : y \mapsto y - \nabla \psi^c(y)$ . Substituting this into the push-forward condition (12) gives, assuming enough regularity of  $\varphi^*$  (see section 5.5),

$$\bar{\rho} = (\rho \circ \nabla \varphi^*) \det D^2 \varphi^*. \quad (39)$$

We omitted the absolute value around the Jacobian determinant since we know  $\varphi^*$  is convex. This PDE is known as the *Monge-Ampère equation*. It is subject to the transport condition  $\nabla\varphi^* : \Omega_2 \rightarrow \Omega_1$ . To fulfil this, it is enough to require that the boundary maps into the boundary,  $\nabla\varphi^* : \partial\Omega_2 \rightarrow \partial\Omega_1$  [46], which is equivalent to the first condition stated above.

As for the second condition, if both  $\rho$  and  $\bar{\rho}$  are bounded from above and below, we can write  $\det D^2\varphi^* = \frac{\bar{\rho}}{\rho \circ \nabla\varphi^*}$  and indeed one can show that  $\varphi$  is strictly convex in this case, as the left hand side is strictly positive (see section 5.5).

A sufficient condition to enforce positivity of the Jacobian determinant  $\det D\Phi^{-1}$  would be that  $\Phi^{-1}(y) = y - \sum_{j=1}^{n_s} \omega_j \nabla\psi_j^c$ ,  $\omega_1, \dots, \omega_{n_s}$  are normalized, non-negative weights, and  $\det(\text{Id} - D^2\psi_{j^*}^c) > 0, \omega_{j^*} > 0$  for at least one  $j^*$ . This is the setting of (L)OT barycenters. In this work, we opt to go for linear combinations over convex ones in order to make use of the POD compression on the tangent space at the cost of guaranteed bijectivity. A similar approach is taken in [43], see section 6.2.

In the entropic case, the transport maps are also gradients of convex functions (remark 7). However, the entropic Monge map does not exactly fulfil the OT boundary condition. This is also the case if the support of  $\bar{\rho}, \rho$  does not coincide with  $\Omega$ .

The boundary condition can be enforced in a post-processing step by  $H^1$ -projecting the  $\psi^c$ . To be precise, we solve the system

$$\begin{aligned} \int_{\Omega} (\kappa^2 \nabla\psi^c \cdot \nabla v + \psi^c v) + \delta^{-1} \int_{\partial\Omega} (\nabla\psi^c \cdot \hat{n}) v \\ = \int_{\Omega} (\kappa^2 \nabla\psi_{\text{pre-proj.}}^c(\mu_i) \cdot \nabla v + \psi_{\text{pre-proj.}}^c(\mu_i) v) \quad \forall v \in V_h \end{aligned} \quad (40)$$

for every  $i = 1, \dots, n_s$ . Here,  $\psi_{\text{pre-proj.}}^c$  denotes the output of the entropic OT calculations and  $\psi^c$  is the projected potential used for the mapping. There are two parameters to set:  $\delta$  is a penalty term to enforce the boundary condition and is set to  $10^{-9}$  in our numerical experiments. The value of  $\kappa$  determines the scale on which the function changes shape to fit the boundary condition. Since we expect the error introduced by the entropic smoothing to be of the scale  $\sqrt{\varepsilon}$  and we want to limit the number of free parameters in our method, we set  $\kappa^2 = \varepsilon^{-1}$ .

**Remark 15.** *If  $\psi_{\text{pre-proj.}}^c$  is very far from fulfilling the boundary conditions, this step can deform the potential to the point that  $y \mapsto \frac{|y|^2}{2} - \psi^c(y)$  is no longer convex and the mapping no longer invertible.*

## 5.5 Regularity of the mapping

The theory on the regularity of OT potentials is an involved topic and a proper treatment is beyond the scope of this work. The interested reader can refer to [49, 21, 46, 5].

In the un-regularized case, the transport potential  $\psi$  from  $\rho$  to  $\sigma$  introduced in Brenier's theorem 1 is differentiable  $\rho$ -almost everywhere as long as  $\rho$  is absolutely continuous with respect to the Lebesgue measure. The brief explanation of this fact is that through the c-transform,  $\psi$  shares the modulus of continuity with the cost function ([39], Section 1.2). Clearly, in our method, we implicitly assume higher regularity of  $\psi$ . This can be argued for with the following result, which is a special case of the regularity theory developed by Caffarelli as presented in [49], Theorem 4.14: When  $\Omega$  is open, bounded, uniformly convex, and of class  $C^{2,\alpha}$ ,  $\rho$  and  $\sigma$  are Hölder continuous functions  $\in C^{0,\alpha}(\bar{\Omega})$ , bounded above and below by positive constants, then the solution  $\varphi$  to the Monge-Ampère eq. (39) is of class  $C^{2,\alpha}(\Omega) \cap C^{1,\alpha}(\bar{\Omega})$ . In particular, through the classical bootstrapping arguments from elliptic regularity,  $\varphi$  is  $C^\infty$  in the interior if  $\rho$  and  $\sigma$  are.

Even in this case, the constants appearing in these estimates can be prohibitively large. Consider the example from proposition 4. As shown in appendix D, the transport map reads  $T_{\rho_{\bar{\mu}} \rightarrow \rho_{\mu}}(y) = 1 - \frac{1}{\mu} \sinh^{-1} \left( \frac{\sinh \frac{\mu}{\bar{\mu}} \sinh(\bar{\mu}(1-y))}{\sinh \bar{\mu}} \right)$  and therefore  $\partial_y T_{\rho_{\bar{\mu}} \rightarrow \rho_{\mu}}(1) \approx \frac{\bar{\mu}}{\mu} e^{\mu - \bar{\mu}}$ , which can take extreme values for typical  $\mu$  and  $\bar{\mu}$ .

For the regularized case, the transport potentials are smooth as they are defined by Gaussian convolutions in eq. (20) and we recall that  $\|\nabla^k \psi\|_\infty = \mathcal{O}(1 + \varepsilon^{1-k})$  [14]. However, the same caveats apply. We ultimately require our regularized transport map to resemble the un-regularized one.

Increasing  $\varepsilon$  too much will degrade the quality of the mapping. The projection step as defined in section 5.4 will preserve the regularity of the potentials (with a constant depending on  $\kappa$ ) as it is an elliptic problem.

In practice, it seems to be effective to increase the lower bound on the densities. For example, when using  $\rho(u) = (1 - s)\frac{u}{f_u} + s$  with  $s > 0$  in proposition 4, we see that the derivative of the transport map is controlled (fig. 2). The entropic smoothing for OT barycenters discussed in section 4.6 can provide this effect.

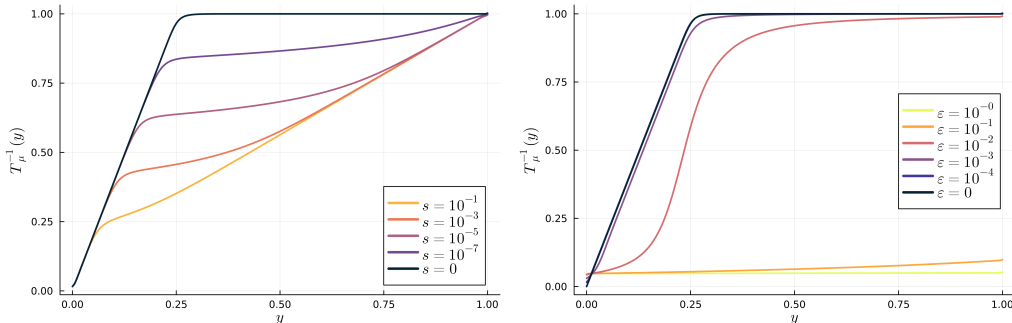


Figure 2: Transport maps for the problem from proposition 4 with  $\varepsilon^2 = 10^{-1}$  and  $\mu_{\min} = 20$ . Left: transport map  $T_{\mu_{\min}}^{-1}$  for different values of  $s$  with  $\varepsilon$  constant at  $10^{-4}$ . Right: different values of  $\varepsilon$  with  $s \equiv 0$ . We see that the parameter  $s$  that sets a lower bound to the densities can control the derivatives of the mapping in this example. Note that modification of  $T$  beyond the point  $x^* \approx \frac{\mu}{\bar{\mu}} \approx 0.26$  does not impact the approximation result in proposition 4 (appendix D) so that the choice  $s = 10^{-7}$  provides the same error bounds while keeping the derivatives of  $T$  and  $T^{-1}$  under control.

Lastly, we have to remark that we cannot directly apply these regularity results to the numerical examples of section 7: our domain is only of class  $C^0$  and the potentials  $\psi$  are approximated using  $H^1$  conforming finite element functions that are only piece-wise  $C^1$ .

## 5.6 Hyper-reduction

When the online phase can be made fully independent of the size  $N$  of the high-fidelity problem, its computational cost can be reduced dramatically. For now, the assembly of linear and bilinear forms has to be done online and depends on  $N$  (remark 13). We can remedy this shortcoming using the *Empirical Interpolation Method* (EIM). In particular, we utilize a version of EIM based on a POD of the parameter-dependent forms [7, 43]. We briefly recall the method using the example of the mapped Laplace operator from eq. (37).

Based on the data from the training set, a collection of snapshots

$$\{[D\Phi_{\mu_i}^{-1}]^{-1}[D\Phi_{\mu_i}^{-1}]^{-T}|\det D\Phi_{\mu_i}^{-1}|\}_{i=1}^{n_s} =: \{K_{\mu_i}\}_{i=1}^{n_s} \quad (41)$$

is used to obtain a POD basis from the correlation matrix  $\mathbb{C}^K : \mathbb{C}_{ij}^K = \int_{\Omega} \text{tr}(K_{\mu_i}^T K_{\mu_j}) dy, 1 \leq i, j \leq n_s$ . Using an energy criterion  $\tau_{\text{eim}}$ , the eigenvectors  $\Xi_q : 1 \leq q \leq Q$  corresponding to the  $Q$  largest eigenvalues are selected to span an approximation space. Coefficients  $\theta_q(\mu)$  and functions  $X_q : 1 \leq q \leq Q$  are determined such that  $K_{\mu} \approx \sum_{q=1}^Q \theta_q(\mu) X_q$  for all  $\mu$ . The way the interpolation points and functions are selected guarantees that the matrix  $B \in \mathbb{R}^{Q \times Q} : B_{q'q} = X_{q'}(y_q^{\text{eim}})$  is lower-triangular with unit diagonal, so the interpolation problem is well-defined and quickly (i.e. in  $\mathcal{O}(Q^2)$  time) solved. The procedure is outlined in appendix C, algorithm 2.

Online,  $K_{\mu}$  is evaluated at select points  $\{y_q^{\text{eim}}\}_{q=1}^Q$  and the interpolation problem  $K_{\mu}(y_q^{\text{eim}}) = \sum_{q'=1}^Q \theta_{q'}(\mu) X_{q'}(y_q^{\text{eim}}) : 1 \leq q \leq Q$  is solved to obtain  $\{\theta_q(\mu)\}_{q=1}^Q$ . The full form  $\int_{\Omega} \nabla \phi_j \cdot K_{\mu} \nabla \phi_j dy$  is approximated using  $\sum_{q=1}^Q \theta_q(\mu) \int_{\Omega} \nabla \phi_j \cdot X_{q,ij} \nabla \phi_j dy$  where the integral defines a  $Q \times n_m \times n_m$  tensor that can be pre-computed offline. As a result, no integration in the high-fidelity space has to be done online. The online cost of the EIM procedure consists of  $Q$  evaluations of  $K_{\mu}$ , the

$\mathcal{O}(Q^2)$  interpolation problem, and a  $\mathcal{O}(Qn_m^2)$  tensor contraction. Importantly, it does not depend on  $N$ . Oversampling techniques which have been shown to improve the stability of the empirical interpolation method in the presence of noisy data [30] are not used in this work.

## 6 Comparison to other works

There have been a number of works that link model order reduction with OT techniques. In this section, we will briefly present some of them and discuss how they relate to the present work.

### 6.1 Optimal transport barycenter coordinates

Recall the definition of an OT barycenter (15):

$$\text{OTBar}(\{\omega_i; \rho_i\}_{i=1}^n) := \arg \min_{\sigma \in \mathcal{P}(\Omega)} \sum_{i=1}^n \omega_i \text{OT}(\rho_i, \sigma)^2.$$

Given a suitable set of probability densities  $\{\rho_1, \dots, \rho_n\}$  denoted *atoms* in the spirit of dictionary learning, for any  $\rho \in \mathcal{P}(\Omega)$ , one can define optimal weights as

$$\{w_i^{\text{opt}}(\rho)\}_{i=1}^n := \arg \min_{\substack{\omega_1, \dots, \omega_n \geq 0 \\ \sum_{i=1}^n \omega_i = 1}} \text{Loss}(\rho, \text{OTBar}(\omega_1, \dots, \omega_n; \rho_1, \dots, \rho_n)), \quad (42)$$

given a suitable loss function  $\mathcal{P}(\Omega) \times \mathcal{P}(\Omega) \rightarrow \mathbb{R}$ . This method yields a parametrization of elements of  $\mathcal{P}(\Omega)$  through a small number of  $n$  non-negative, normalized weights.

In [4], the authors apply this procedure to several application cases from computer graphics to medical imaging. The optimal weights are called *barycenter coordinates* and different loss functions are used. The optimization problem (42) is solved using a standard L-BFGS quasi-Newton solver.

A different approach is proposed in [52]. Therein, the authors use the fact that at the minimum defining the OT barycenter 15, the Fréchet derivative of  $\sigma \mapsto \sum_{i=1}^n \omega_i \text{OT}(\rho_i, \sigma)^2$  has to be zero. Under mild assumptions outlined in their work, it holds that  $\nabla_{\sigma} \sum_{i=1}^n \omega_i \text{OT}(\rho_i, \sigma)^2 = -\sum_{i=1}^n \omega_i (T_{\sigma \rightarrow \rho_i} - \text{id}) = \sum_{i=1}^n \omega_i \nabla \psi_{\sigma \rightarrow \rho_i}$ . One obtains a quadratic optimization problem on the simplex of normalized weights featuring a correlation matrix as introduced in definition 14:

$$\left\| \nabla_{\rho} \sum_{i=1}^n \omega_i \text{OT}(\rho_i, \rho)^2 \right\|_{L^2(\rho)}^2 = \sum_{i,j=1}^n \omega_i \omega_j \langle \nabla \psi_{\rho \rightarrow \rho_i}, \nabla \psi_{\rho \rightarrow \rho_j} \rangle_{L^2(\rho)} \stackrel{!}{=} 0, \quad (43)$$

subject to  $\omega_1, \dots, \omega_n \geq 0, \sum_{i=1}^n \omega_i = 1$ .

In the later works [25, 41], the authors do not work with a given set of atoms, but instead determine them by optimization: given a training set  $\{\rho_i\}_{i=1}^{n_s}$ , the optimization problem reads

$$\min_{\substack{\omega_j(\rho_i) \geq 0 \forall i,j \\ \sum_{i=j}^n \omega_j(\rho_i) = 1 \forall i \\ \sigma_1, \dots, \sigma_n \in \mathcal{P}(\Omega)}} \sum_{i=1}^{n_s} \text{Loss}(\rho_i, \text{OTBar}(\{\omega_j(\rho(i)); \sigma_j\}_{j=1}^n)). \quad (44)$$

Equations (42) and especially (44) are complicated multilevel optimization problems, which however can be tackled using a tailored warm-start technique as outlined in Section 4.2 of [41]. The gradients involved can either be computed from closed formulas provided therein, or using automatic differentiation techniques. However, even with those adaptations, solving for truly optimal barycentric weights online remains computationally restrictive.

Another option to construct the set of atoms  $\{\sigma_i\}_{i=1}^n$  is through greedy algorithms, see [3, 12]. Promoting sparsity in the weight vectors  $\{\omega_i\}_{i=1}^n$  is beneficial to memory footprint and run-time cost on the one hand, and mitigates issues of possible redundancy in the set of atoms on the other hand [10, 25].

Most of the works mentioned utilize entropic regularisation to make the OT computations feasible, except for [12, 3], where the authors apply barycentric approximations to one-dimensional

PPDE problems. In one spatial dimension, there is a closed formula available for the transport from  $\rho$  to  $\sigma$ , given by their cumulative distribution functions (cdf):

$$T_{\rho \rightarrow \sigma} = \text{cdf}(\sigma)^{[-1]} \circ \text{cdf}(\rho). \quad (45)$$

The superscript  $[-1]$  denotes the pseudo-inverse as defined in chapter 2 of [39]. Note that for the case  $\Omega = [0, 1]$  and  $\bar{\rho} = \mathbb{1}_{[0,1]}$ , the inverse cdf operation coincides with the Monge embedding:  $T_{\bar{\rho} \rightarrow \sigma} = \text{cdf}(\sigma)^{[-1]}$ . The method of *tangent principal component analysis* (tPCA) [12] on the set of  $\{\text{cdf}(\rho(\mu_i))^{[-1]}\}_{i=1}^{n_s}$ , which proved numerically unstable, is a special case of performing a POD on the Monge embeddings.

Convex displacement interpolation (CDI), introduced in [19], is based on a linear approximation of the displacement interpolation between two measures. The CDI method is non-intrusive and similar in spirit to the barycentric coordinates. In order to solve the OT problems needed to build the displacement interpolations, the authors rely on the closed form available for the OT between multivariate Gaussian densities [31]. See also [37], where displacement interpolation is used to interpolate between solutions of PPDEs at different parameter values.

OT barycentric coordinates have proven effective at parametrizing sets of probability densities in numerous applications. One drawback of these methods, however, is that it is very hard to go beyond interpolation-based methods in the online phase. The reconstruction  $\omega_1(\mu), \dots, \omega_n(\mu) \mapsto \text{OTBar}(\mu)$  is costly and non-linear, complicating the online evaluation of a PDE residual such as  $\|\mathcal{L}(\text{OTBar}(\mu); \mu)\|_{L^2}$ .

Methods based on OT barycenters are inherently limited when it comes to extrapolation tasks (see [3], section 5.3). We avoid this limitation in our work by moving to the tangent space of  $\mathcal{P}(\Omega)$  and replacing the convex combinations with linear ones.

## 6.2 Registration methods

As discussed in section 3, the principle of recasting PPDE problems using parametric mappings  $\Phi_\mu$  in order to obtain a mapped solution manifold  $\Phi_\mu(\mathcal{M}) = \{u(\mu) \circ \Phi_\mu^{-1} : u(\mu) \in \mathcal{M}\}$  that is better suited for linear reduction techniques, has been studied extensively. As an example, we will discuss the method presented in [43, 45]. Therein, mappings of the form

$$y \mapsto y + \sum_{j=1}^{m^{\text{hf}}} w^{\text{hf}}(\mu)_j \chi_j^{\text{hf}}(y) \quad (46)$$

are proposed. As in section 5,  $w^{\text{hf}}(\mu)_{1, \dots, m^{\text{hf}}} \in \mathbb{R}$  are parameter-dependent coefficients, while  $\chi_{1, \dots, m^{\text{hf}}}^{\text{hf}}$  are elements of a general approximation space such as Legendre polynomials or Fourier expansions. The mappings are constructed such that

$$\left\| u(\mu) \circ \left( y + \sum_{j=1}^{m^{\text{hf}}} w^{\text{hf}}(\mu)_j \chi_j^{\text{hf}}(y) \right) - \bar{u} \right\| \quad (47)$$

is small, given a reference  $\bar{u}$ . Besides this *proximity measure*, the optimization penalizes the  $H^2$  seminorm of the mappings and enforces certain constraints to keep the Jacobian of the mappings strictly positive. To guarantee a sufficiently rich set of mappings to optimize over,  $m^{\text{hf}}$  has to be rather large, which can be restrictive when evaluating mappings in the online phase. Consequently, the authors also opt for a POD approach, reducing the number of mapping terms to  $m$  based on an eigenvalue decomposition of the matrix with elements  $\mathbb{C}^w = \{w^{\text{hf}}(\mu)_i \cdot w^{\text{hf}}(\mu)_j\}_{1 \leq i, j \leq m^{\text{hf}}}$ . This method is similar to the one we propose in the present work. Note that also in this case, it cannot be guaranteed that this approximate mapping is invertible, even if the high fidelity one is. However, the method proved stable in the numerical test cases considered.

In [44], figure 5, the authors show the performance of a registration method based on a non-linear optimization problem when using a general polynomial space  $\{\chi_j^{\text{hf}}\}_{j=1}^{m^{\text{hf}}}$  and a space comprised only of gradient functions, i.e.  $\chi_j^{\text{hf}} = \nabla \psi_j^{\text{hf}} : 1 \leq j \leq m^{\text{hf}}$  of similar dimension. Methods that rely on transport maps to approximate  $\Phi$  are by construction confined to the latter

space. In this example, it is shown that while the performance is very similar for small and medium deformations, the optimization method using gradient functions deteriorates for large deformations, leading to  $\sim 10\times$  higher iteration numbers and even inverted elements (i.e. non-bijective  $\Phi$ ). The method proposed in this work cannot be directly applied to this test case, as it is a point registration problem and un-regularized OT gives no guarantees of invertible mappings when the transported measures give mass to small sets.

In [18], the authors propose a snapshot registration method based on *advection modes*, which are obtained using the matrix  $\{\text{OT}(\rho(\mu_i), \rho(\mu_j))\}_{1 \leq i, j \leq n_s}$  and applying techniques of Euclidean distance matrix methods [11]. The mapping of the snapshots is done in the sense of push-forward measures, that is

$$\rho(\mu) \approx (\bar{\rho} \circ \Phi_\mu + r(\mu) \circ \Phi_\mu) \det D\Phi_\mu. \quad (48)$$

Here,  $r(\mu)$  denotes a residual term that needs to be determined in the online phase. Especially in the case where  $u$  itself is used to construct the transport mappings, this would be a natural choice for our method as well, since the transport mappings are constructed to fulfil this push-forward relation. Up to numerical inaccuracies, we would expect  $n_m = 1$ .

We chose the form eq. (34), which corresponds to the push-forward of a function, for two reasons: First, the relation  $\bar{\rho} = \rho(\mu_i) \circ (\text{id} - \nabla\psi^c(\mu_i)) \det(\text{Id} - D^2\psi^c(\mu_i)) \forall i$  only holds if the transport mappings are constructed directly from  $u$  itself and not another derived quantity  $\rho(u)$ . Second, substituting the push-forward relation for a density into a PDE residual requires evaluating derivatives of  $\det(\text{Id} - D^2\psi^c)$ , which requires even more regularity of  $\psi^c$ , and higher order basis functions in the discretization.

To summarize, our work aims to hit a compromise between interpolating methods based on optimal transport and registration approaches. By using linear OT and transforming our snapshots as functions, not densities, we accept the need for more reference basis functions  $\phi_{1, \dots, n_m}$  in return for a lower-order residual that has to be evaluated in the online phase.

## 7 Numerical experiments

We will demonstrate the proposed method and the impact of some of the hyperparameters on two test cases. For the Finite Element calculations, we rely on the `Gridap.jl` library<sup>1</sup> [47, 2], while Gaussian processes are calculated using `GaussianProcesses.jl`<sup>2</sup>. The computational OT routines used are available in the package `WassersteinDictionaries.jl`<sup>3</sup>.

### 7.1 Poisson’s equation with moving source

Let  $\Omega = [0, 1]^2$ , discretized by a  $64 \times 64$  grid of quadrilateral cells. For  $V_h$ , we chose  $H_0^1$ -conforming Legendre basis functions of order  $p = 3$ , which leads to  $N = 36481$  degrees of freedom. The grid size is denoted with  $h$ . The equation we solve is

$$\Delta u(x; \mu) = f(x; \mu) : x \in \Omega, u(x; \mu) = 0 : x \in \partial\Omega, \quad (49)$$

where  $f$  is a narrow Gaussian with variance  $\text{var} = 10^{-3}$  and mean  $(\frac{1}{2}, \frac{1}{2}) + \mu$ ,  $\mu \in (-\frac{7}{20}, \frac{7}{20})^2 = \mathcal{A}$ .

To construct the mappings and reduced basis we draw  $n_s = 100$  samples of  $\mu$  uniformly from  $\mathcal{A}$ . The solutions to this equation are not probability densities, so we use  $\rho(u)(\mu) = \frac{u(\mu)^2}{\int u(\mu)^2}$  and  $\rho(u)(\mu) = f(\mu)$  to calculate the transport mappings. These computations, which rely on collocation, are performed on a finer  $192 \times 192$  grid of quadrilaterals. The iterative OT solver is set to stop when the  $l_1$  error of the marginal constraint reaches  $10^{-3}$  or at the maximum number of iterations of  $\lceil \frac{10}{\epsilon} \rceil$ . As reference density  $\bar{\rho}$  we chose the OT barycenter of the training snapshot densities. Note that it is not crucial for the proposed method to use the OT barycenter. Any reference density, even  $\bar{\rho} \equiv |\Omega|^{-1}$ , can be used. However, when  $\bar{\rho}$  is an average of the data  $\{\rho(\mu_i)\}_{i=1}^{n_s}$  in a meaningful sense (which the OT barycenter is in these cases), we expect the transport maps to have a simpler structure and require fewer modes  $m$  to approximate. We

<sup>1</sup><https://github.com/gridap/Gridap.jl>

<sup>2</sup><https://github.com/STOR-i/GaussianProcesses.jl>

<sup>3</sup><https://github.com/JuliaRCM/WassersteinDictionaries.jl>

employ an annealing strategy as described in [13], section 3.3.3, initializing the regularization parameter to one and then halving it at every iteration until we reach  $\varepsilon$ . To invert the mapping at the last step, we use the c-transform with  $\varepsilon_{\text{fine}} = \frac{h^2}{10}$ .

Given a threshold  $\tau(\mathcal{E})$ ,  $m$  is chosen such that  $1 - \mathcal{E}(m; \lambda) < \tau$ , where

$$\mathcal{E}(m; \lambda) := \frac{\sum_{i=1}^m \lambda_i}{\sum_{j=1}^{\text{rank } \mathbb{C}} \lambda_j}. \quad (50)$$

We set  $\tau_{\text{eim}} = \frac{\tau}{10}$  to account for the difficulty in approximating the moving source term.

The Gaussian process we use is taken as-is from the reference package. In particular, we select a zero mean function, a squared exponential kernel with characteristic length and standard deviation set to one (the default settings). The log standard deviation of observation noise is set to  $-6$ . These parameters have not been optimized.

### 7.1.1 The case $\rho(u)(\mu) \propto u(\mu)^2$

Since  $\rho(\mu)$  is positive on all of  $\Omega$  in this case, we use de-biased calculations, replacing  $\text{OT}_\varepsilon$  with  $S_\varepsilon$  when needed. The transport maps are now given by the de-biased potentials as defined in eq. (28). We see that de-biasing improves the performance of the method, both by increasing the accuracy and by reducing the number of approximation functions  $n_m$  and  $Q$ , in table 2.

Figure 3 displays the eigenvalue decay for the correlation matrices of snapshots  $\mathbb{C}^u$ , transported snapshots  $\mathbb{C}^{\Phi_*u}$ , and Monge embeddings  $\mathbb{C}^\psi$ . As expected, the eigenvalues of the mapped snapshots are indicative of a much faster  $n$ -width decay of  $\Phi_\mu(\mathcal{M})$  compared to that of  $\mathcal{M}$ .

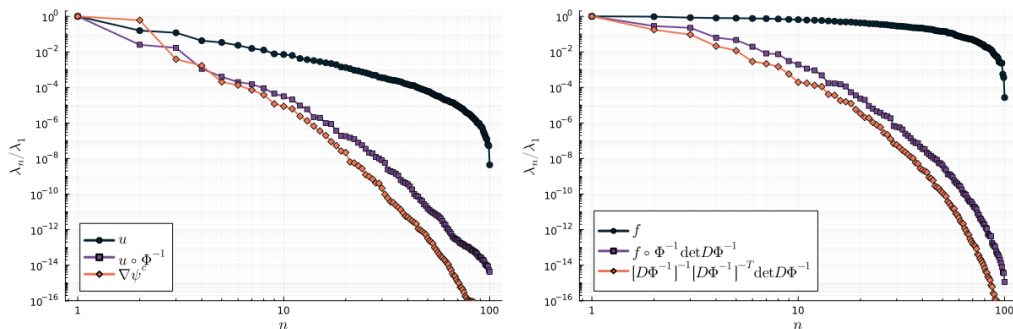


Figure 3: Left: Eigenvalues of the correlation matrices  $\mathbb{C}^u$ ,  $\mathbb{C}^{\Phi_*u}$ , and  $\mathbb{C}^\psi$ . Right: Eigenvalues of the correlation matrices  $\mathbb{C}^f$ ,  $\mathbb{C}^K$ , and  $\mathbb{C}^{\Phi_*f}$  used in the hyper-reduction.  $\varepsilon = 10^{-2}$ ,  $\tau = 10^{-4}$ ,  $\rho(u)(\mu) \propto u(\mu)^2$ , and de-biasing are used.

Figure 4 shows the first four transport modes  $\xi_{1,\dots,4}^c$  and the Gaussian process approximations of  $\mu \mapsto w_j(\mu)$ , the transport mode coefficients used in the mapping  $\Phi_\mu^{-1} = \text{id} - \nabla \sum_{j=1}^m w_j(\mu) \xi_j^c$ . The first two modes are essentially translations, the third mode is a contraction (or expansion, depending on the sign of its coefficient), and the fourth mode is a contraction along one diagonal and an expansion along the other.

As indicated by the very fast eigenvalue decay of the correlation matrix  $\mathbb{C}^\psi$ , transport mappings can be approximated accurately as a linear combination of only a few transport modes. Next, we compare the error in the solution of the PPDE for the entire online phase. This includes approximating the mapping with transport modes, obtaining the coefficients of the transport modes with a Gaussian process, solving the PPDE in the reference domain as in (37), and mapping the solution back to the physical domain as in (34). Average and maximum errors are calculated for a test set using  $n_t = 50$  samples from  $\mathcal{A}$ . The results are compared to the classical POD method with no registration step, i.e. the  $m = 0$  case. The hyper-reduction uses EIM to evaluate the mapped Laplacian as described in section 5.6 as well as the right-hand-side term  $\int_\Omega \phi_i f_\mu \det D\Phi_\mu^{-1} dy \forall i = 1, \dots, n_m$ . The number of interpolation functions are denoted  $Q_K$  and  $Q_f$ , respectively. Values for the cases of  $m = 0$  using hyper-reduction are not given,



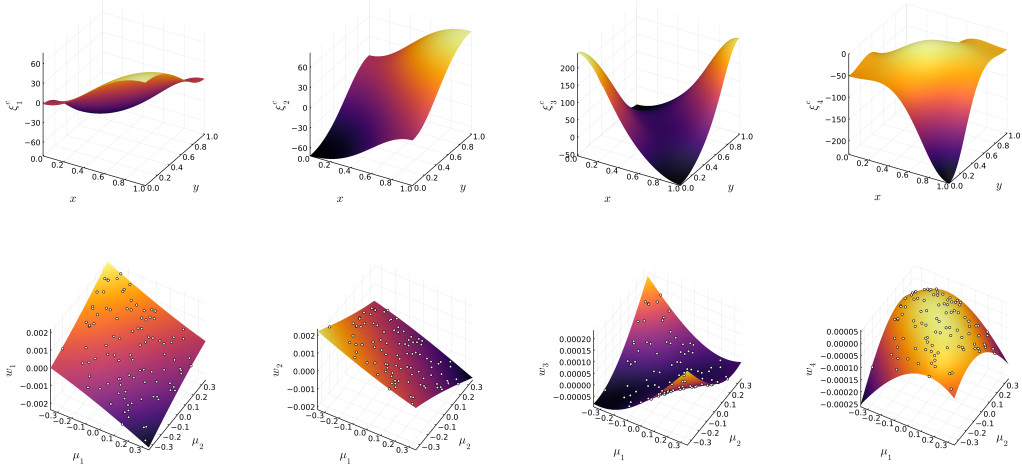


Figure 4: First row: first four transport modes with an added constant such that  $\xi_{1,\dots,4}^c(\frac{1}{2}, \frac{1}{2}) = 0$ . Second row: Gaussian process approximation of the functions  $w_{1,\dots,4}(\mu)$ . Values used to construct the basis are marked in white. The parameters chosen as in fig. 3.

since the set  $\{f(\mu)\}_{\mu \in \mathcal{A}}$  shows extremely slow  $n$ -width decay. In contrast, the  $n$ -width decay of  $\{f(\mu) \circ \Phi_\mu^{-1} \det D\Phi_\mu^{-1}\}_{\mu \in \mathcal{A}}$  allows the use of EIM albeit with large values of  $Q_f$ .

We also report the relative error of the  $H^1$  semi-norm of  $u(\mu)$ , i.e. the error in the energy of the solution for an electrostatic problem. We choose this as an example of a quantity of interest that can be computed in the reference domain.

$\tau(\mathcal{E})$	$n$	$m$	$Q_K$	$Q_f$	relative $L^2$ error of $u(\mu)$		relative $H^1$ error of $u(\mu)$		relative error of $\ u(\mu)\ _{\dot{H}^1}$	
					avg	max	avg	max	avg	max
$10^{-3}$	41	0	-	-	$7.87 \times 10^{-2}$	$3.32 \times 10^{-1}$	$2.99 \times 10^{-1}$	$7.08 \times 10^{-1}$	$1.09 \times 10^{-1}$	$5.07 \times 10^{-1}$
	5	4	-	-	$4.48 \times 10^{-2}$	$1.27 \times 10^{-1}$	$9.80 \times 10^{-2}$	$2.16 \times 10^{-1}$	$1.11 \times 10^{-2}$	$4.67 \times 10^{-2}$
	5	4	12	19	$4.94 \times 10^{-2}$	$1.25 \times 10^{-1}$	$1.02 \times 10^{-1}$	$2.20 \times 10^{-1}$	$2.12 \times 10^{-2}$	$7.13 \times 10^{-2}$
$10^{-4}$	64	0	-	-	$5.85 \times 10^{-2}$	$3.19 \times 10^{-1}$	$2.28 \times 10^{-1}$	$6.93 \times 10^{-1}$	$7.75 \times 10^{-2}$	$4.85 \times 10^{-1}$
	9	6	-	-	$1.53 \times 10^{-2}$	$4.04 \times 10^{-2}$	$4.27 \times 10^{-2}$	$1.01 \times 10^{-1}$	$1.71 \times 10^{-3}$	$8.20 \times 10^{-3}$
	9	6	19	24	$1.67 \times 10^{-2}$	$5.10 \times 10^{-2}$	$4.42 \times 10^{-2}$	$1.08 \times 10^{-1}$	$8.17 \times 10^{-3}$	$4.70 \times 10^{-2}$
$10^{-5}$	82	0	-	-	$5.10 \times 10^{-2}$	$2.99 \times 10^{-1}$	$2.02 \times 10^{-1}$	$6.71 \times 10^{-1}$	$6.68 \times 10^{-2}$	$4.55 \times 10^{-1}$
	11	10	-	-	$7.23 \times 10^{-3}$	$2.36 \times 10^{-2}$	$2.79 \times 10^{-2}$	$6.20 \times 10^{-2}$	$5.43 \times 10^{-4}$	$2.32 \times 10^{-3}$
	11	10	28	30	$9.88 \times 10^{-3}$	$5.23 \times 10^{-2}$	$3.02 \times 10^{-2}$	$9.15 \times 10^{-2}$	$6.26 \times 10^{-3}$	$5.31 \times 10^{-2}$

Table 1: PPDE solution errors in the test set as a function of the retained eigenvalue energy for  $\varepsilon = 10^{-2}$ ,  $\rho(\mu) \propto u(\mu)^2$ , and de-biased calculations.

de-biasing	$n$	$m$	$Q_K$	$Q_f$	relative $L^2$ error of $u(\mu)$		relative $H^1$ error of $u(\mu)$		relative error of $\ u(\mu)\ _{\dot{H}^1}$	
					avg	max	avg	max	avg	max
yes	9	6	-	-	$1.53 \times 10^{-2}$	$4.04 \times 10^{-2}$	$4.27 \times 10^{-2}$	$1.01 \times 10^{-1}$	$1.71 \times 10^{-3}$	$8.20 \times 10^{-3}$
	9	6	19	24	$1.67 \times 10^{-2}$	$5.10 \times 10^{-2}$	$4.42 \times 10^{-2}$	$1.08 \times 10^{-1}$	$8.17 \times 10^{-3}$	$4.70 \times 10^{-2}$
no	10	7	-	-	$1.52 \times 10^{-2}$	$5.42 \times 10^{-2}$	$4.89 \times 10^{-2}$	$1.02 \times 10^{-1}$	$2.61 \times 10^{-3}$	$9.97 \times 10^{-3}$
	10	7	15	35	$1.97 \times 10^{-2}$	$8.00 \times 10^{-2}$	$5.19 \times 10^{-2}$	$1.18 \times 10^{-1}$	$1.22 \times 10^{-2}$	$5.27 \times 10^{-2}$

Table 2: PPDE solution errors in the test set with and without de-biasing, using  $\varepsilon = 10^{-2}$ ,  $\tau = 10^{-4}$ ,  $\rho(\mu) \propto u(\mu)^2$ .

In order to see how much of the overall error of the method is made when inverting  $\Phi_\mu^{-1}$ , we compare  $u_{\text{trb}} \circ \Phi_\mu^{-1}$  to  $u \circ \Phi_\mu^{-1}$  in the case  $\tau = 10^{-5}$  and using hyper-reduction. Calculating the approximation error in the reference domain in this way, we find average and maximum  $L^2$  errors of  $9.31 \times 10^{-3}$  and  $5.62 \times 10^{-2}$ . The average and maximum  $H^1$  errors are  $2.13 \times 10^{-2}$  and  $8.61 \times 10^{-2}$ . We conclude that the approximation error in the reference domain dominates in the overall error of the method. For some parameter values, the two can even compensate each other.

### 7.1.2 The case $\rho(u)(\mu) = f(\mu)$

This case is added here to see how well the effect of entropic smoothing can be used to apply the method even when  $\rho$  takes very small values in  $\Omega$ . In this case, we do not use de-biased potentials and barycenters. Indeed, when using de-biased quantities, the performance of the method is heavily degraded with this choice of  $\rho$ .

As expected, there are only three eigenvalues of  $\mathbb{C}^\psi$  different from machine zero in this case - corresponding to two translations and one scaling mode (i.e.  $y \mapsto \text{const.} \cdot y^2$ ) which is a consequence of the entropic smoothing. The eigenvalue decay of  $\mathbb{C}^K$  and  $\mathbb{C}^{\Phi_* f}$  is also improved (fig. 5). Approximation errors for this case are shown in table 3 and are comparable to the case  $\rho(u) \propto u^2$  even at  $m = 3$ . However, note that the online cost is mostly dependent on  $n$ , not  $m$ , see section 7.1.4.

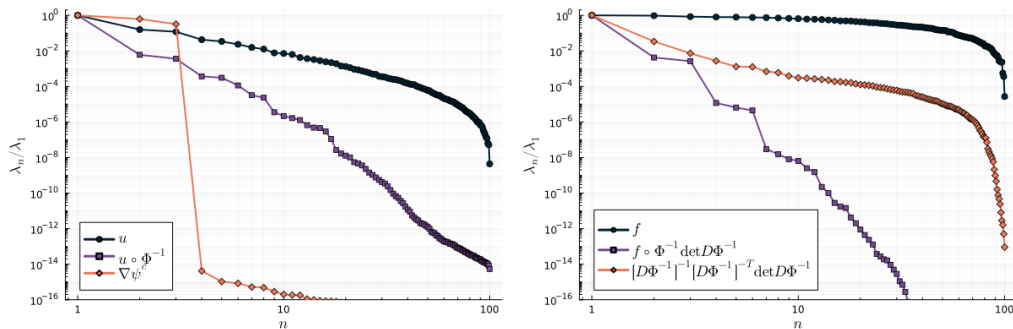


Figure 5: Left: Eigenvalues of the correlation matrices  $\mathbb{C}^u$ ,  $\mathbb{C}^{\Phi_* u}$ , and  $\mathbb{C}^\psi$  for the case  $\rho(\mu) = f(\mu)$ . Right: Eigenvalues of the correlation matrices  $\mathbb{C}^f$ ,  $\mathbb{C}^K$ , and  $\mathbb{C}^{\Phi_* f}$  used in the hyper-reduction. No de-biasing,  $\varepsilon = 10^{-2}$ ,  $\tau = 10^{-4}$ ,  $\rho(\mu) = f(\mu)$ .

$\tau(\mathcal{E})$	$n$	$m$	$Q_K$	$Q_f$	relative $L^2$ error of $u(\mu)$		relative $H^1$ error of $u(\mu)$		relative error of $\ u(\mu)\ _{\tilde{H}^1}$	
					avg	max	avg	max	avg	max
$10^{-3}$	41	0	-	-	$7.87 \times 10^{-2}$	$3.32 \times 10^{-1}$	$2.99 \times 10^{-1}$	$7.08 \times 10^{-1}$	$1.09 \times 10^{-1}$	$5.07 \times 10^{-1}$
	3	3	-	-	$7.46 \times 10^{-2}$	$2.03 \times 10^{-1}$	$1.33 \times 10^{-1}$	$2.68 \times 10^{-1}$	$1.81 \times 10^{-2}$	$6.76 \times 10^{-2}$
	3	3	9	12	$7.84 \times 10^{-2}$	$2.17 \times 10^{-1}$	$1.35 \times 10^{-1}$	$2.69 \times 10^{-1}$	$1.58 \times 10^{-2}$	$9.24 \times 10^{-2}$
$10^{-4}$	64	0	-	-	$5.85 \times 10^{-2}$	$3.19 \times 10^{-1}$	$2.28 \times 10^{-1}$	$6.93 \times 10^{-1}$	$7.75 \times 10^{-2}$	$4.85 \times 10^{-1}$
	6	3	-	-	$3.00 \times 10^{-2}$	$8.91 \times 10^{-2}$	$8.03 \times 10^{-2}$	$1.24 \times 10^{-1}$	$4.00 \times 10^{-3}$	$1.32 \times 10^{-2}$
	6	3	12	19	$3.00 \times 10^{-2}$	$8.10 \times 10^{-2}$	$8.08 \times 10^{-2}$	$1.28 \times 10^{-1}$	$8.68 \times 10^{-3}$	$4.49 \times 10^{-2}$
$10^{-5}$	82	0	-	-	$5.10 \times 10^{-2}$	$2.99 \times 10^{-1}$	$2.02 \times 10^{-1}$	$6.71 \times 10^{-1}$	$6.68 \times 10^{-2}$	$4.55 \times 10^{-1}$
	9	3	-	-	$1.09 \times 10^{-2}$	$2.75 \times 10^{-2}$	$6.69 \times 10^{-2}$	$9.01 \times 10^{-2}$	$1.73 \times 10^{-3}$	$5.74 \times 10^{-3}$
	9	3	15	26	$1.27 \times 10^{-2}$	$3.85 \times 10^{-2}$	$6.73 \times 10^{-2}$	$9.31 \times 10^{-2}$	$5.38 \times 10^{-3}$	$4.09 \times 10^{-2}$

Table 3: PPDE solution errors in the test set as a function of the retained eigenvalue energy. No de-biasing,  $\varepsilon = 10^{-2}$ ,  $\tau = 10^{-4}$ ,  $\rho(\mu) = f(\mu)$ .

Again, we compute the error in the reference domain to estimate the error induced by inverting the mapping. Using hyper-reduction, the average  $L^2$  error is  $6.71 \times 10^{-3}$  with a maximum of  $2.76 \times 10^{-2}$ . For the  $H^1$  error, we find  $1.60 \times 10^{-2}$  and  $4.91 \times 10^{-2}$ . We conclude that the error contributions are of the same order of magnitude in this case.

### 7.1.3 Influence of the smoothing parameter

The parameter  $\varepsilon$  influences the method in two ways. Firstly, it acts as a hyper-parameter to balance fidelity and regularity of the mapping  $\Phi$  itself. Secondly, when using  $\bar{\rho} = \text{OTBar}_\varepsilon\{\rho_i\}_{i=1}^{n_s}$ ,  $\varepsilon$  influences the shape of  $\bar{\rho}$ . Especially with no de-biasing, the entropic bias (see section 4.6) leads to a smoothing of  $\bar{\rho}$ .

When  $\rho(\mu) \propto u(\mu)^2$ , the densities are supported on the full domain and we vary  $\varepsilon$  for all calculations. We report results in fig. 6 for the case with no de-biasing. The results for the de-biased case are very similar. We give the error in the reference domain here to separate the effect of inaccuracies when inverting  $\Phi_\mu^{-1}$ .

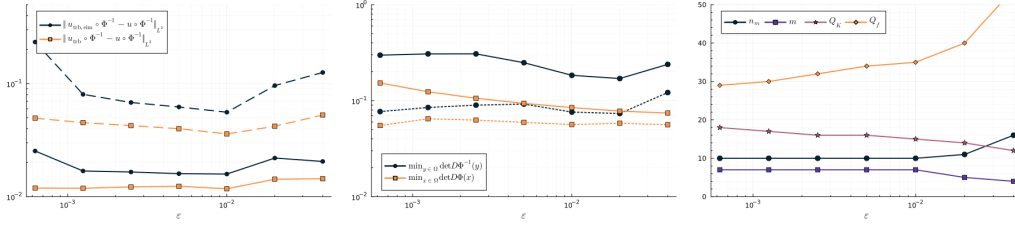


Figure 6: Influence of the regularisation parameter  $\varepsilon$ . In all cases,  $\tau = 10^{-4} = 10\tau_{\text{eim}}$ ,  $\rho(\mu) \propto u(\mu)^2$ , and no de-biasing was used. Left: relative average (solid) and maximum (dashed)  $L^2$  error over the test set. Middle: minimum value of the determinant of the mapping and its inverse: average (solid) and minimum (dotted) over  $\mu \in \mathcal{A}_{\text{test}}$ . The inverse mapping is calculated using the entropic c-transform with  $\varepsilon_{\text{fine}}$ . Right: number of approximation modes.

Firstly and importantly, we observe that the approximation quality does not strongly depend on  $\varepsilon \in [10^{-3}, 10^{-2}]$ . Reducing  $\varepsilon$  significantly below  $10^{-3}$  would require all OT calculations to be moved to the log-domain, as  $\min_{x,y} \exp \frac{-c(x,y)}{\varepsilon}$  becomes numerically zero in double precision.

As  $\varepsilon$  becomes too large, the empirical interpolation method does not work as well any more, as the source terms  $\{f(\mu_i)\}_i$  are no longer well aligned, leading to an increase in  $Q_f$ . As discussed in section 5.4, the mapping can even be non-invertible in these cases. Note that the value  $\varepsilon = 4 \times 10^{-2}$  corresponds to a characteristic scale of the transport of  $\sqrt{\varepsilon} = 0.2$ .

#### 7.1.4 Run times

The codebase used to generate the results presented in this work is still being developed and parts of it have not yet been optimized. Thus, a thorough treatment of runtimes is beyond the scope of this work. Comparisons between the high-fidelity solver, the POD method, and the presented method depend on the size of high fidelity simulation  $N$ , the size of training- and test-set  $n_s$  and  $n_t$ , and several other factors. Depending on the choice of these parameters, one or another method might seem favourable. Regardless, we show some examples in table 4. The parameters chosen in these runs are a subset of those in table 1 and table 3, where the corresponding errors can be found.

We clearly see the additional cost induced by the transport and registration. Hyper-reduction leads to large computational speed-up ( $\approx 100$  to  $200$ ) in the online phase by removing the dependence on  $N$ . We also see that  $n_m$  has a larger impact on the cost of the method than  $m$ . The post-processing step to map the solutions back to the physical domain is costly, as it again depends on the size of the full order model.

In several applications, this last step is not needed. Quantities of interest can be obtainable in the reference domain, so the inversion of  $\Phi_\mu^{-1}$  is not necessary. For example, the energy  $\frac{1}{2} \int \nabla u \cdot \nabla u$  that we report here, or other linear functionals of the form  $l(u) = \int u f_l$  can be calculated in the reference domain with no cost depending on the dimension of the full problem. For time-dependent problems, mapping back to the physical domain is only needed for diagnostics and plotting of the solution and thus usually not done at every time-step.

## 7.2 Non-linear advection equation

As a second test case, we consider the equation

$$\partial_t u(x, t) + \bar{a}(\theta) \cdot \nabla (u(x, t) + \gamma u(x, t)^2) = \beta \Delta u(x, t), \quad (51)$$

where  $x \in \Omega = [0, 1]^2$  and  $t \in [0, T]$ . The advecting velocity is given by  $\bar{a}(\alpha) = \frac{1}{5}(\cos \alpha, \sin \alpha)$ , depending on the parameter  $\alpha \in [0, 2\pi]$ . The strength of the non-linearity is set to  $\gamma = 10^{-2}$  and  $\beta$  is set to  $10^{-3}$ . The parameter space is therefore  $\mathcal{A} := [0, 1] \times [0, 2\pi] \ni (t, \alpha) = \mu$ . As an initial condition, we choose a Gaussian centred at  $(\frac{1}{2}, \frac{1}{2})$  with a variance of  $5 \times 10^{-3}$ . The solution is discretized using the same basis as in the previous example on a coarser  $32 \times 32$  grid of

					offline phase I: transport calculations (all $\mu \in \mathcal{A}_{\text{train}}$ )			
			OT barycenter and potentials	boundary projection	transport modes	mapped snapshots		
$\rho(\mu)$	$\bar{\rho}$ and $\{\psi_{\text{pre-proj.}}^c(\mu_i)\}_{i=1}^{n_s}$		$\{\psi^c(\mu_i)\}_{i=1}^{n_s}$	$\{\xi_j^c\}_{j=1}^m$	$\{u(\mu_i) \circ \Phi_{\mu_i}^{-1}\}_{i=1}^{n_s}$			
$\propto u(\mu)^2$	27s		19s	33s	43s			
$f(\mu)$	6.6s		19s	33s	43s			

					offline phase II (all $\mu \in \mathcal{A}_{\text{train}}$ )				
			gaussian process	reduced basis	assembly	hyper-reduction			
$\rho(\mu)$	$n$	$m$	$Q_K$	$Q_f$	$\{w(\mu)\}_{i=1}^m$	$\{\zeta_i\}_{i=1}^n$ or $\{\phi_i\}_{i=1}^{n_m}$	$\int \nabla \zeta_i \cdot \nabla \zeta_j$	EIM $_K$	EIM $_f$
none	64	-	-	-	-	19s	9.4s	-	-
	82	-	-	-	-	18s	15s	-	-
$\propto u(\mu)^2$	10	7	19	24	2.3s	18s	-	86	42s
	11	10	28	30	3.6	17s	-	93s	50s
$f(\mu)$	6	3	12	19	1.3s	18s	-	83s	43s
	9	3	12	19	1.2s	18s	-	86s	43s

					online (per $\mu \in \mathcal{A}_{\text{test}}$ )		post-processing (per $\mu \in \mathcal{A}_{\text{test}}$ )		
					no EIM	EIM	re-mapping		
$\rho(\mu)$	$n$	$m$	$Q_K$	$Q_f$	$u_{\text{rb}}$ or $u_{\text{trb}} \circ \Phi_{\mu}^{-1}$	$u_{\text{trb}} \circ \Phi_{\mu}^{-1}$	$[\sum_{j=1}^m w_j(\mu) \xi_j^c]_{\text{pre-proj.}}$	$\Phi(\mu)$	$u_{\text{trb}}(\mu)$
none	64	-	-	-	0.14s	-	-	-	-
	82	-	-	-	0.17s	-	-	-	-
$\propto u(\mu)^2$	10	7	19	24	0.71s	4.9ms	0.24s	0.19s	0.41s
	11	10	28	30	0.95s	5.5ms	0.24s	0.20s	0.41s
$f(\mu)$	6	3	12	19	0.43s	4.5ms	0.24s	0.19s	0.40s
	9	3	15	26	0.71s	5.1ms	0.24s	0.19s	0.41s

Table 4: Run times for different choices of  $\rho$ . Parameters are as in table 1 and table 3.

quadrilaterals, using  $N = 9025$  degrees of freedom. Time-integration is performed by an implicit midpoint method with time-step  $\Delta t = 5 \times 10^{-2}$ .

The reduced basis and transport modes are computed using the solutions at every time-step in  $[0, T^{\text{train}} = \frac{4}{5}]$  for ten different values of  $\alpha$  on a uniform grid between 0 and  $2\pi$ , thus  $n_s = 170$ . The solutions  $u$  themselves are used as the densities  $\rho(u) = u$  for the OT computations, which are performed on a  $96 \times 96$  grid. We set  $\varepsilon = 10^{-2}$  and use the OT barycenter of the training set as a reference density. No de-biasing is used. We let  $\tau_{\text{eim}} = \tau = 10^{-3}$ . All other parameters are identical to the previous example.

The selected energy criterion leads to  $n = 24$  for the classical RB method and  $n_m = 5, m = 3$  for the proposed one. For the hyper-reduction, the RB method with  $m = 0$  requires only an EIM approximation for  $\bar{a}$ , which can be done to machine precision with  $Q = 2$  modes. The method with transport requires EIM approximations for  $\det D\Phi_{\mu}^{-1}$ ,  $D\Phi_{\mu}^{-1} \partial_t \Phi_{\mu}^{-1} \det D\Phi_{\mu}^{-1}$ ,  $D\Phi_{\mu}^{-1} \bar{a}(\mu) \det D\Phi_{\mu}^{-1}$ , and  $[D\Phi_{\mu}^{-1}]^{-1} [D\Phi_{\mu}^{-1}]^{-T} \det D\Phi_{\mu}^{-1}$ . The values of  $Q$  for these terms are 4, 4, 3, and 4, respectively. The corresponding eigenvalue decays are shown in fig. 7.

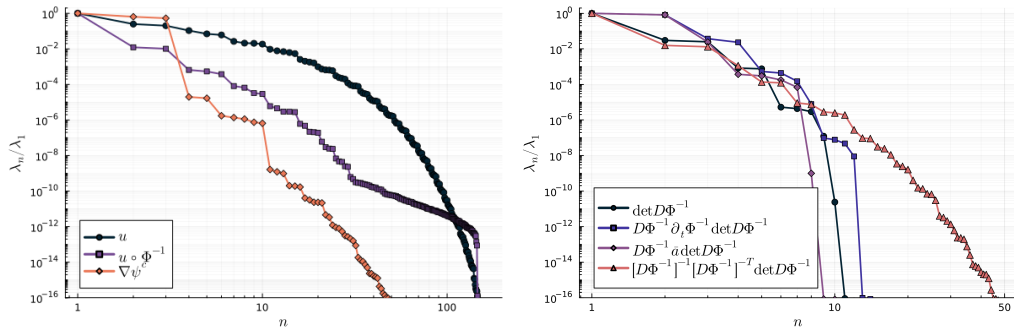


Figure 7: Left: Eigenvalues of the correlation matrices  $\mathbb{C}^u$ ,  $\mathbb{C}^{\Phi^*u}$ , and  $\mathbb{C}^\psi$ . Right: Eigenvalues of the correlation matrices used in the hyper-reduction.

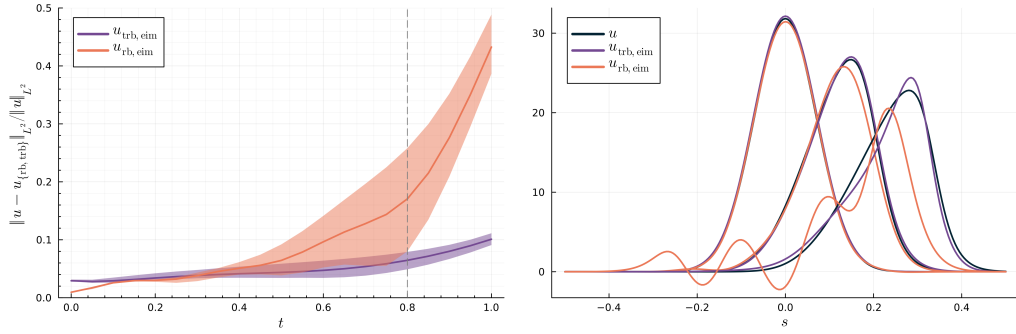


Figure 8: Left: Relative  $L^2$  errors for the non-linear advection-diffusion equation as a function of time. Plotted is the average error across all ten values of  $\alpha$ . The shaded area is bounded above and below by the maximum and minimum error. The dashed line indicates  $T^{\text{train}}$  and the beginning of the extrapolation region. Right: cross-sections in propagation direction (parameterized by  $s$ ) for the value of  $\alpha$  where the proposed method performs the worst and for  $t \in \{0, \frac{1}{2}, 1\}$ .

Figure 8 shows the relative  $L^2$  errors over time for 20 values of  $\alpha$  randomly chosen from  $[0, 2\pi]$  and for  $t \in [0, T^{\text{test}} = 1]$ . The average approximation  $L^2$  error of  $\{u(T^{\text{test}}, \alpha_j)\}_{1 \leq j \leq 10}$  in the proposed method is  $1.01 \times 10^{-1}$ , while the maximum is  $1.11 \times 10^{-2}$ . We see that the classical RB method is only accurate for solutions close to the initial condition and for some select values of  $\alpha$  close to those in the training set. This issue cannot be remedied by adding more reduced basis functions, since the solutions for values of  $\alpha$  not in the training set and  $t > T^{\text{train}}$  cannot be expressed by any linear combination of training snapshots. In contrast, the proposed method yields qualitatively correct results even with the low number of modes employed.

## 8 Summary

In this work, we presented a data-driven registration method based on Monge embeddings. In the simple numerical examples we considered, the method proved robust and showed the expected improvements compared to an approach without registration.

Several possible extensions and open questions regarding the method have been mentioned throughout the text. For example, would be desirable to enforce the mapping boundary conditions in the construction itself instead of a later projection step. Furthermore, the OT computations, which rely mostly on convolution operations, could be performed in the same finite element framework as the PPDE solution itself. In the present work, the potentials are represented by  $H^1$  conforming finite element functions, which are crucially not of class  $C^1$ . We would expect the method to profit from a  $C^2$  conforming approximation, e.g. using a spectral polynomial basis.

Due to the parameter-dependence of the mapped forms, hyper-reduction methods are crucial to make the method performant in the online phase. Several other hyper-reduction methods exist that have been applied successfully in many applications, such as the empirical quadrature method [53].

The method requires three central inputs from the user: An entropic regularization parameter  $\varepsilon$ , a energy cut-off criterion  $\tau$ , and a choice of density  $\rho$ . In order to stay close to the true OT problem,  $\varepsilon$  should be chosen small, keeping in mind that the transport plan will essentially ignore all features smaller than  $\sqrt{\varepsilon}$ . The choice of  $\tau$  depends on the desired accuracy versus cost of the approximation. Selecting  $\rho$  is the most intricate issue (of course, if the PPDE solution itself is a probability density, this is a natural choice). For maximum robustness,  $\rho$  should be bounded from below on the entire domain by a positive constant. The size of this constant can have a significant effect on  $\|\Phi_\mu\|$  as discussed in section 5.5. The numerical experiments indicate that entropic smoothing of the reference density can make the method applicable in some cases where  $\rho$  takes very small values in the domain.

## 9 Acknowledgements

The presented work is supported by the Helmholtz Association and the Munich School of Data Science.

We would like to thank Michael Kraus and Olga Mula for stimulating discussions about the method and its numerical implementation.

## A Notation

The following table repeats some of the notation that is repeatedly used throughout the article:

$\langle \cdot, \cdot \rangle_H$	inner product in the Hilbert space $H$
$.*, ./, \dots$	element-wise operations, e.g. $(\hat{a}.*\hat{b})_i = \hat{a}_i * \hat{b}_i$ ;
$(\cdot)$	collocated quantity $\hat{a}_i = a(x_i)$
$\oplus$	notation for $(\psi_\rho \oplus \psi_\sigma)(x, y) = \psi_\rho(x) + \psi_\sigma(y)$
$(\cdot)_\#$	push-forward operation for a density, see eq. (12)
$(\cdot)^*$	Legendre transform $f^*(y) := \sup_x (\langle x, y \rangle - f(x))$
$\mathbb{1}$	indicator function: $\mathbb{1}_{\Omega'}(x) = 1$ if $x \in \Omega'$ and zero otherwise
$\mathcal{A}$	parameter space
$B$	interpolation matrix used in empirical interpolation, see section 5.6
$c$	cost function $c(x, y) = \frac{1}{2} x - y ^2$
$(\cdot)^c$	c-transform, see definition 5
$\mathbb{C}^u$	correlation matrix of $u_1, \dots, u_{n_s}$ , see definition 2
$\mathcal{C}_b$	space of bounded continuous functions
cdf	cumulative distribution function
$\mathcal{E}(n; \lambda)$	retained eigenvalue energy, see eq. (50)
$h$	grid width
id, Id	identity $x \mapsto x$ , identity matrix
$k$	Gibbs kernel $k(x, y) = \exp(-\frac{1}{\varepsilon}c(x, y))$
$\mathcal{L}(\cdot; \mu)$	parameter-dependent PDE operator $V_h \rightarrow \mathbb{R}$
$m$	number of transport modes, see definition 14
$\mathcal{M}$	solution manifold, see eq. (2)
$\max_{(\cdot) \sim u}^\varepsilon, \min_{(\cdot) \sim u}^\varepsilon$	softmax and softmin operations, see definition 12
$n, n_m$	number of reduced basis functions, see definition 2 and eq. (34)
$n_s, n_t$	number of snapshots in the training and test set
$N$	dimension (i.e. number of degrees of freedom) of the high fidelity discretization
$\mathcal{N}$	normal distribution
$\mathcal{P}$	set of probability measures
$\text{LOT}(\rho, \sigma)$	Linear Optimal Transport distance between $\rho$ and $\sigma$ , see definition 9
$\mathcal{O}$	$f = \mathcal{O}(1 + x^k) \Leftrightarrow f$ is bounded by an order $k$ polynomial with positive coefficients
$\text{OT}(\rho, \sigma)$	Optimal Transport or Wasserstein distance between $\rho$ and $\sigma$ , see definition 3
$\text{OTBar}, \text{LOTBar}$	(Linear) Optimal Transport barycenter, see definition 7 and definition 10
$Q$	number of EIM modes, see section 5.6.
$T$	Transport or Monge map, see eq. (14)
$u, v$	elements of $V_h$
$\tilde{u}$	coefficients used to approximate $u_{\text{trb}}$ , see eq. (34)
$v$	matrix eigenvector
$V_h$	discretized function space
$w$	transport mapping coefficient, see section 5.1
$X$	EIM mode, see section 5.6
$\delta$	penalization parameter, set to $10^{-9}$ or smaller
$\varepsilon$	entropic regularization parameter, see eq. (18)
$\varepsilon_{\text{fine}}$	regularization used when inverting $\Phi^{-1}$ . Set to the order of $h^2$ .
$\zeta$	POD basis function, see definition 2

$\theta$	EIM coefficients, see section 5.6.
$\kappa$	$H^1$ projection parameter, see section 5.4. Set to $\varepsilon^{-1/2}$
$\lambda$	matrix eigenvalue, non-increasing: $\lambda_1 \geq \lambda_2 \geq \dots$
$\mu$	parameter in $\mathcal{A}$
$\pi$	transport plan, see eq. (7)
$\Pi(\rho, \sigma)$	set of admissible transport plans between $\rho$ and $\sigma$ , see eq. (8)
$\rho, \sigma$	probability densities
$\bar{\rho}$	reference density, see definition 8 and section 5.1
$\varsigma$	measure used in the regularisation term of entropic OT, see eq. (18)
$\tau, \tau_{\text{eim}}$	energy criterion for POD: $1 - \mathcal{E}(n; \lambda) < \epsilon$ defines $n$
$\varphi$	$x \mapsto \frac{ x ^2}{2} - \psi(x)$ , see theorem 1
$\phi$	POD basis function in the reference domain, see eq. (34)
$\Phi_\mu$	parameter-dependent mapping, see eq. (6)
$\xi^c$	transport mode, see definition 14
$\Xi$	POD modes used in the EIM construction, see section 5.6
$\psi$	transport potential, see eq. (9)
$\omega$	barycenter weight, see definition 7.
$\Omega$	physical domain $\subset \mathbb{R}^d$

## B Optimal transport computations

In this section, we will provide some details on how we compute the OT ingredients from Section 5. The routines are available in the package `WassersteinDictionaries.jl`<sup>4</sup>.

### B.1 Sinkhorn's algorithm

We rely on the tools from entropic OT for our computations. In order to not needlessly bloat the notation, we will omit the superscript  $\varepsilon$  from the entropic transport potential  $\psi^\varepsilon$  and Monge map  $T^\varepsilon$ . Furthermore, we will write  $N$  (rather than  $N_{\text{fine}}$ ) for the dimension of the discrete problem, which does not necessarily coincide with the dimension of the discrete space used to approximate the PPDE solution.

Using the regularized formulation of OT allows us to leverage very fast algorithms developed in recent years, which we repeat for convenience. Suppose that the quantities are discretized by collocation, i.e.  $\hat{\rho}_i = \rho(x_i) : 1 \leq i \leq N$ ,  $\hat{\sigma}_i = \sigma(x_i) : 1 \leq i \leq N$ , and  $\hat{C}_{ij} = c(x_i, y_j) : 1 \leq i, j \leq N$ . Algorithm 1 exclusively relies on element-wise operations and matrix-vector products. The Ma-

---

#### Algorithm 1 Sinkhorn's algorithm

---

```

1: function SINKHORN( $\hat{\rho}, \hat{\sigma}, \hat{C}, \varepsilon, \text{tol}$ )
2:    $\hat{a}, \hat{b} \leftarrow 1$  ▷ . denotes element-wise operations
3:    $\hat{K} \leftarrow \exp.(-\varepsilon^{-1}\hat{C})$ 
4:   while  $\|\hat{\rho} - \hat{\rho}.*\hat{a}.*\hat{K}(\hat{b}.*\hat{\sigma})\|_1 > \text{tol}$  do ▷  $L^1$  error of the marginal condition
5:      $\hat{a} \leftarrow 1 ./ \hat{K}(\hat{b}.*\hat{\sigma})$ 
6:      $\hat{b} \leftarrow 1 ./ \hat{K}(\hat{a}.*\hat{\rho})$ 
7:   end while
8:   return  $\varepsilon \log.\hat{a}, \varepsilon \log.\hat{b}$  ▷ The Kantorovich potentials
9: end function

```

---

trix  $\hat{C}$  can be evaluated lazily, which reduces the memory footprint from  $N^2$  to  $N$ . However, the quantities  $\hat{K}$ ,  $\hat{a}$ , and  $\hat{b}$  become numerically unstable as  $\varepsilon \rightarrow 0$ .

A very similar algorithm can be used to calculate OT barycenters. In the case of the barycenters, even moderate values of  $\varepsilon > 0$  cause a blurring of the result, which can be corrected by using a slightly modified algorithm (see also Section 4.6). Our implementation follows [20] and we refer

<sup>4</sup><https://github.com/JuliaRCM/WassersteinDictionaries.jl>

to this work for further details.

## B.2 Log-domain c-transform

For many applications, moderate values of  $\varepsilon$  might be sufficient (around  $10^{-3}$  in our numerical examples) and Algorithm 1 can be run without numerical over- or underflow. However, in our approach, there is one step that relies on  $\varepsilon$  to be very small, say of order  $10^{-6}$ : The approximation of the c-transform to invert the transport mappings. For this, we rely on the softmin function (22):

$$\hat{\psi}_j^{c,\varepsilon} := -\varepsilon \log \sum_{i=1}^N \exp\left(\frac{\hat{\psi}_i^\varepsilon - \hat{C}_{ij}}{\varepsilon}\right) \hat{\rho}_i \quad 1 \leq j \leq N. \quad (52)$$

The non-zero weights  $\hat{\rho}_i$  can be absorbed in the exponent as  $\exp \log \hat{\rho}_i$ , obtaining a *LogSumExp* operation. This is a standard function implemented in many programming languages and can be calculated very accurately, without round-off errors, using only a single pass over  $i$ . We use the implementation from the package `LogExpFunctions.jl`<sup>5</sup>.

## B.3 Seperable kernels

Naive implementations of both the matrix-vector products from Algorithm 1 and the *LogSumExp* evaluation in (52) are of  $\mathcal{O}(N^2)$  complexity due to nested loops over  $i$  and  $j$ . Note that  $N$  scales exponentially with the spatial dimension of the problem when it is discretized on a grid. However, in the special case of  $c(x, y) = \frac{1}{2}|x - y|^2$  we are working with, we can do better, as pointed out in [42]. Note that in dimension  $d$ , the cost is separable in  $d$  terms along each dimension:  $\frac{1}{2}|x - y|^2 = \frac{1}{2}|x^1 - y^1|^2 + \dots + \frac{1}{2}|x^d - y^d|^2$ . Now assume the points  $x_i$  are sampled on a regular tensor grid and therefore can be indexed as  $x_{i_1, \dots, i_d} : 1 \leq i_1, \dots, i_d \leq N^{1/d}$ . Note that  $x_{i_1, \dots, i_d}^l$  can be denoted with  $x_{i_l}^l$ , as only the  $l$ th coordinate changes when varying the indices  $i_1, \dots, i_d$ . Let  $\hat{c}_{ij}^l := |x_{i_l}^l - y_{j_l}^l|^2$  and  $\hat{k}^l = \exp(-\hat{c}^l/\varepsilon)$ . In this case,

$$\begin{aligned} (\hat{K}\hat{a})_j &= \sum_{1 \leq i \leq N} \hat{K}_{ij} \hat{a}_i \\ \Leftrightarrow (\hat{K}\hat{a})_{j_1, \dots, j_d} &= \sum_{1 \leq i_1, \dots, i_d \leq N^{1/d}} \hat{k}_{i_1 j_1} \cdots \hat{k}_{i_d j_d} \hat{a}_{i_1, \dots, i_d} \\ &= \sum_{1 \leq i_1 \leq N^{1/d}} \hat{k}_{i_1 j_1} \cdots \sum_{1 \leq i_d \leq N^{1/d}} \hat{k}_{i_d j_d} \hat{a}_{i_1, \dots, i_d} \end{aligned} \quad (53)$$

As a result, instead of computing one large matrix-vector product of complexity  $N^2$ , we are computing  $d$  tensor contractions of complexity  $N^{1+1/d}$  each. An analogous trick can be applied in the log-domain as well.

In order to utilize this separable kernel trick, when it comes to the OT calculations, we sample the densities  $\rho$  on a fine, regular tensor grid and perform the calculations as outlined above. This yields point-wise approximations to the Kantorovich potentials  $\{\psi(x_i), \psi^c(y_i)\}_{i=1}^N$ . In order to obtain the transport map  $T$  and its Jacobian  $DT$ , we use this data to construct finite element approximations to  $\psi$  and  $\psi^c$  in  $V_h$ . Note that we could also use a different approximation space at this point.

## C EIM algorithm

For convenience, we give the full algorithm to construct an empirical interpolation approximation from section 5.6:

<sup>5</sup><https://github.com/JuliaStats/LogExpFunctions.jl>



---

**Algorithm 2** Empirical Interpolation Method algorithm
 

---

```

1: function EMPIRICALINTERPOLATION( $\{\Xi_q\}_{q=1}^Q$ )
2:   for  $q = 1, \dots, Q$  do
3:     if  $q$  is 1 then
4:        $r \leftarrow \Xi_q$ 
5:     else
6:        $\theta \leftarrow B^{-1} [\Xi_q(y_1^{\text{eim}}), \dots, \Xi_q(y_{q-1}^{\text{eim}})]$ 
7:        $r \leftarrow \Xi_q - \theta \cdot X$ 
8:     end if
9:      $y_q^{\text{eim}} \leftarrow \arg \max_{y \in \Omega} \|r(y)\|_\infty$ 
10:     $X_q \leftarrow r_q / r_q(y_q^{\text{eim}})$ 
11:     $B_{q,q'} \leftarrow X_q(y_{q'}^{\text{eim}}) \quad \forall q' = 1, \dots, Q$      $\triangleright B$  is lower-triangular with unit diagonal.
12:  end for
13:  return  $\{X_q\}_{q=1}^Q, \{y_q^{\text{eim}}\}_{q=1}^Q, B$      $\triangleright$  The interpolation functions, points, and matrix.
14: end function

```

---

## D An analytical example in one dimension

In this section we will show how the method proposed in section 5 performs in a one-dimensional example where analytical solutions can be calculated. The example is taken from appendix B of [43].

**Proposition 5.** *The solutions to the equation*

$$-\partial_{xx}^2 u_\mu + \mu^2 u_\mu = 0 \quad (54)$$

on the domain  $\Omega = (0, 1)$  with boundary conditions  $u_\mu(0) = 1, u_\mu(1) = 0$  and  $\mu, \bar{\mu} \in [\mu_{\min}, \mu_{\max}] =: \mathcal{A}$ ,  $\mu_{\max} = \epsilon^{-2} \mu_{\min}$ ,  $\mu_{\min} > 1$ ,  $\epsilon \in (0, 1)$  satisfy

$$\|u_{\bar{\mu}} - u_\mu \circ T_{\rho_{\bar{\mu}} \rightarrow \rho_\mu}\|_{L^2(\Omega)} \leq \left| \frac{1}{\cosh \mu} - \frac{1}{\cosh \bar{\mu}} \right| \leq 2e^{-\mu_{\min}}, \quad (55)$$

where  $\rho(u) = \frac{u}{f_u}$ .

*Proof.* The solution manifold is given by  $\mathcal{M} = \left\{ \frac{\cosh(\mu(1-x))}{\cosh \mu} : \mu \in \mathcal{A} \right\}$ . In this one-dimensional example, the OT maps can be calculated analytically using cumulative density functions. Since  $\rho(u) = \frac{u}{f_u}$ ,  $\rho(u_\mu) =: \rho_\mu = \mu \frac{\cosh(\mu(1-x))}{\sinh \mu}$ . Furthermore,  $\text{cdf}(\rho_\mu)(x) = 1 - \frac{\sinh(\mu(1-x))}{\sinh \mu}$ ,  $\text{cdf}(\rho_\mu)^{[-1]}(p) = 1 - \frac{1}{\mu} \sinh^{-1}((1-p) \sinh \mu)$ , and

$$T_{\rho_{\bar{\mu}} \rightarrow \rho_\mu}(y) = \text{cdf}(\rho_\mu)^{[-1]} \circ \text{cdf}(\rho_{\bar{\mu}})(y) = 1 - \frac{1}{\mu} \sinh^{-1} \left( \frac{\sinh \mu}{\sinh \bar{\mu}} \sinh(\bar{\mu}(1-y)) \right). \quad (56)$$

The map  $T_{\rho_{\bar{\mu}} \rightarrow \rho_\mu}$  is a bijection as it is strictly increasing and  $T_{\rho_{\bar{\mu}} \rightarrow \rho_\mu}(\partial\Omega) = \partial\Omega$ . The former is a consequence of  $0 < \rho_\mu < +\infty \forall \mu$ .

Using  $\cosh \circ \sinh^{-1}(x) = \sqrt{1+x^2}$ , and letting  $z = \bar{\mu}(1-y)$ , we write

$$\|u_{\bar{\mu}} - u_\mu \circ T_{\rho_{\bar{\mu}} \rightarrow \rho_\mu}\|_{L^2(\Omega)}^2 = \frac{1}{\bar{\mu}} \int_0^{\bar{\mu}} \frac{1}{\cosh \mu^2} \left( \frac{\cosh \mu}{\cosh \bar{\mu}} \cosh z - \sqrt{1 + \frac{\sinh \mu^2}{\sinh \bar{\mu}^2} \sinh z^2} \right)^2 dz \quad (57)$$

where  $\sinh z^2$  denotes  $(\sinh z)^2$ . We can check using symbolic numerical software that the integrand has no local maximum, as any stationary condition at  $z \neq 0$  requires either  $\frac{\sinh \mu^2}{\sinh \bar{\mu}^2} < \frac{\cosh \mu}{\cosh \bar{\mu}} < \frac{\sinh \mu}{\sinh \bar{\mu}} \Leftrightarrow \frac{\sinh \mu}{\sinh \bar{\mu}} < \frac{\tanh \bar{\mu}}{\tanh \mu} < 1$  or the same relation will all inequalities reversed, either of which lead to contradiction for  $\mu, \bar{\mu} > 0$ . As the integrand vanishes at  $z = \bar{\mu}$ , its maximum value is attained at  $z = 0$ , i.e.  $y = 1$ , and we find

$$\|u_{\bar{\mu}} - u_\mu \circ T_{\rho_{\bar{\mu}} \rightarrow \rho_\mu}\|_{L^2(\Omega)} \leq |\Omega| |u_{\bar{\mu}}(1) - u_\mu \circ T_{\rho_{\bar{\mu}} \rightarrow \rho_\mu}(1)| = \left| \frac{1}{\cosh \bar{\mu}} - \frac{1}{\cosh \mu} \right|. \quad (58)$$

□

**Remark 16.** If we chose  $\bar{\rho} = \text{OTBar}\{\rho_\mu : \mu \in \mathcal{A}\}$  with uniform weights, we find  $\bar{\rho} = \rho_{\bar{\mu}}$  with  $\bar{\mu} = \frac{\mu_{\max} - \mu_{\min}}{\log \mu_{\max} - \log \mu_{\min}}$ , the logarithmic mean. The choice made in [43] is  $\bar{\mu} = \sqrt{\mu_{\min} \mu_{\max}}$ .

**Remark 17.** Note that  $T_{\rho_{\bar{\mu}} \rightarrow \rho_\mu}(y) \approx T_{\rho_{\bar{\mu}} \rightarrow \rho_\mu}(0) + y \partial_y T_{\rho_{\bar{\mu}} \rightarrow \rho_\mu}(0) = \frac{\bar{\mu}}{\mu} \frac{\tanh \mu}{\tanh \bar{\mu}} y \approx \frac{\bar{\mu}}{\mu} y$  and this approximation is close until either  $y \approx \frac{\bar{\mu}}{\mu}$  (when  $\mu < \bar{\mu}$ ) or  $y \approx 1$  (when  $\mu > \bar{\mu}$ ).

The derivative of  $T_{\rho_{\bar{\mu}} \rightarrow \rho_\mu}$  can take extreme values:  $\partial_y T_{\rho_{\bar{\mu}} \rightarrow \rho_\mu}(1) = \frac{\bar{\mu}}{\mu} \frac{\sinh \mu}{\sinh \bar{\mu}} \approx \frac{\bar{\mu}}{\mu} e^{\mu - \bar{\mu}}$ .

We now give the proof of proposition 4:

*Proof.* We want to show that (c.f. eq. (36))

$$\inf_{\xi_1^c \in \text{span}\{\psi_\mu^c : \mu \in \mathcal{A}\}} \sup_{\mu \in \mathcal{A}} \inf_{\substack{w_1(\mu) : \Phi^{-1}(y) = y - w_1(\mu) \partial_y \xi_1^c(y) \\ \Phi_\mu^{-1} : \Omega \rightarrow \Omega \text{ is a bijection}}} \|u_{\bar{\mu}} - u_\mu \circ \Phi_\mu^{-1}\|_{L^2(\Omega)} \leq e^{-\mu_{\min}} (4 + \epsilon).$$

By remark 16,  $\bar{\rho} = \rho_{\bar{\mu}}$  with  $\bar{\mu} = \frac{\mu_{\max} - \mu_{\min}}{\log \mu_{\max} - \log \mu_{\min}}$ . Let  $c(\mu) = \frac{\bar{\mu} - \mu}{\mu}$  and  $w(\mu) = -\frac{c(\mu)}{c(\mu_{\min})}$ . We will show the bound by evaluating it at the trial function

$$\Phi_\mu^{-1}(y) := y - w(\mu) \left( T_{\rho_{\bar{\mu}} \rightarrow \rho_{\mu_{\min}}}(y) - y \right), \quad (59)$$

i.e.  $\partial_y \xi_1^c(y) := T_{\rho_{\bar{\mu}} \rightarrow \rho_{\mu_{\min}}}(y) - y$ . Note that, by the properties of the logarithmic mean,  $\frac{\mu_{\min}}{\epsilon} \leq \bar{\mu} \leq \frac{\mu_{\min}}{2\epsilon^2}$ . As a consequence,  $-1 \leq w(\mu) \leq \epsilon$ . As  $T_{\rho_{\bar{\mu}} \rightarrow \rho_{\mu_{\min}}}$  is concave,  $\Phi_\mu^{-1}$  is concave for  $\mu < \bar{\mu}$  and convex otherwise. Consequently,  $\Phi_\mu^{-1}$  is strictly increasing, with  $\partial_y \Phi_\mu^{-1}(y) \geq \partial_y \Phi_{\mu_{\min}}^{-1}(1) > \frac{\bar{\mu}}{\mu_{\min}} e^{\mu_{\min} - \bar{\mu}}$  for  $\mu < \bar{\mu}$  and  $\partial_y \Phi_\mu^{-1}(y) \geq \Phi_{\mu_{\max}}^{-1}(0) \geq \epsilon$  for  $\mu \geq \bar{\mu}$ .

Let  $\delta' := \frac{\mu_{\min}}{\bar{\mu}}$  and write

$$\begin{aligned} \|u_{\bar{\mu}} - u_\mu \circ \Phi_\mu^{-1}\|_{L^2(\Omega)}^2 &\leq \int_0^{\delta'} \left( u_{\bar{\mu}}(y) - u_\mu \circ \frac{\bar{\mu}}{\mu} y \right)^2 dy \\ &\quad + \int_0^{\delta'} \left( u_\mu \circ \Phi_\mu^{-1}(y) - u_\mu \circ \frac{\bar{\mu}}{\mu} y \right)^2 dy + \int_{\delta'}^1 \left( u_{\bar{\mu}}(y) - u_\mu \circ \Phi_\mu^{-1}(y) \right)^2 dy. \end{aligned} \quad (60)$$

For the first term, we can simplify  $|u_{\bar{\mu}}(y) - u_\mu \circ \frac{\bar{\mu}}{\mu} y| = \sinh(\bar{\mu} y) |\tanh \bar{\mu} - \tanh \mu| \leq 2 \sinh(\mu_{\min}) |e^{-2\mu} - e^{-2\bar{\mu}}| \leq e^{-\mu_{\min}} \forall y \in [0, \delta']$ .

For the second term, since  $\Phi_\mu^{-1}$  is either concave or convex, we find that  $|\frac{\bar{\mu}}{\mu} y - \Phi_\mu^{-1}(y)| \leq |\frac{\bar{\mu}}{\mu} y - \partial_y \Phi_\mu^{-1}(0) y| \leq |\frac{\bar{\mu}}{\mu} - 1 + w(\mu) \frac{\bar{\mu}}{\mu_{\min}} \frac{\tanh \mu_{\min}}{\tanh \bar{\mu}} - w(\mu)| \frac{\mu_{\min}}{\bar{\mu}} = |w(\mu)| \left( 1 - \frac{\tanh \mu_{\min}}{\tanh \bar{\mu}} \right) \forall y \in [0, \delta']$ . Therefore,

$$\left| u_\mu \circ \Phi_\mu^{-1}(y) - u_\mu \circ \frac{\bar{\mu}}{\mu} y \right|_{0 \leq y \leq \delta'} \leq \mu \underbrace{\max_{0 \leq y \leq \delta'} \frac{\sinh(\mu(1-y))}{\cosh \mu}}_{=\tanh \mu} |w(\mu)| \left( 1 - \frac{\tanh \mu_{\min}}{\tanh \bar{\mu}} \right). \quad (61)$$

Using the bounds on  $w(\mu)$ ,  $\bar{\mu}$ , and  $1 - \tanh \mu \leq 2e^{-2\mu}$ , this expression is bounded by  $\bar{\mu} \cdot 1 \cdot 1 \cdot 2e^{-2\mu_{\min}} = 2\bar{\mu}e^{-2\mu_{\min}}$  for  $\mu \leq \bar{\mu}$  and  $\mu_{\max} \cdot 1 \cdot \epsilon \cdot 2e^{-2\mu_{\min}} \leq 2\bar{\mu}e^{-2\mu_{\min}}$  otherwise.

For the third term, assume  $\mu \leq \bar{\mu}$ . Recall that in this case,  $\Phi_\mu^{-1}(y) \leq \frac{\bar{\mu}}{\mu} y$  and therefore  $u_\mu \circ \frac{\bar{\mu}}{\mu} y \leq u_\mu \circ \Phi_\mu^{-1}(y)$ . Since the mapping is increasing, the maximum of the integrand is reached at  $y = \delta'$ . We find the following chain of inequalities:  $u_{\bar{\mu}}(\delta') = \cosh \mu_{\min} - \tanh \bar{\mu} \sinh \mu_{\min} \leq \cosh \mu_{\min} - \tanh \mu \sinh \mu_{\min} = u_\mu \circ \frac{\bar{\mu}}{\mu} \delta' \leq u_\mu \circ \Phi_\mu^{-1}(\delta')$ . Lastly, using  $T_{\rho_{\bar{\mu}} \rightarrow \rho_{\mu_{\min}}}(\delta') = 1 - \frac{1}{\mu_{\min}} \sinh^{-1} \left( \frac{\sinh \mu_{\min}}{\sinh \bar{\mu}} \sinh(\bar{\mu} - \mu_{\min}) \right) \geq 1 - \frac{1}{\mu_{\min}}$ , we arrive, after some simplifications, at  $\mu(1 - \Phi_\mu^{-1}(\delta')) \leq \mu - \mu_{\min} + \frac{\bar{\mu} - \mu}{\bar{\mu} - \mu_{\min}} \leq \mu - \mu_{\min} + 1$  and  $u_\mu \circ \Phi_\mu^{-1}(\delta') \leq \cosh(\mu_{\min} - 1) - \sinh(\mu_{\min} - 1) \tanh \mu = e^{1 - \mu_{\min}} + \sinh(\mu_{\min} - 1)(1 - \tanh \mu)$  and therefore

$$|u_{\bar{\mu}}(\delta') - u_\mu \circ \Phi_\mu^{-1}(\delta')| \leq u_\mu \circ \Phi_\mu^{-1}(\delta') \leq e^{1 - \mu_{\min}} + e^{\mu_{\min} - 1} e^{-2\mu} \leq e^{-\mu_{\min}} (e + e^{-1}). \quad (62)$$

When  $\mu \geq \bar{\mu}$ , the reversed inequalities hold and we obtain  $|u_{\bar{\mu}}(\delta') - u_\mu \circ \Phi_\mu^{-1}(\delta')| \leq u_{\bar{\mu}} \circ \Phi_{\bar{\mu}}^{-1}(\delta') = \cosh \mu_{\min} - \sinh \mu_{\min} \tanh \bar{\mu} \leq 2e^{-\mu_{\min}}$ .

Collecting all terms, we find

$$\|u_{\bar{\mu}} - u_\mu \circ \Phi_\mu^{-1}\|_{L^2(\Omega)} \leq \delta' e^{-\mu_{\min}} + \delta' 2\bar{\mu} e^{-2\mu_{\min}} + (1 - \delta')(e + e^{-1}) e^{-\mu_{\min}} < e^{-\mu_{\min}} (4 + \epsilon), \quad (63)$$

using  $0 < \delta' = \frac{\mu_{\min}}{\bar{\mu}} < \epsilon$  and  $\mu_{\min} > 1$ .  $\square$

## References

- [1] L. AMBROSIO, N. GIGLI, AND G. SAVARÉ, *Gradient Flows*, Lectures in Mathematics ETH Zürich, Birkhäuser-Verlag, Basel, 2005, <https://doi.org/10.1007/b137080>.
- [2] S. BADIA AND F. VERDUGO, *Gridap: An extensible Finite Element toolbox in Julia*, JOSS, 5 (2020), p. 2520, <https://doi.org/10.21105/joss.02520>.
- [3] B. BATTISTI, T. BLICKHAN, G. ENCHÉRY, V. EHRLACHER, D. LOMBARDI, AND O. MULA, *Wasserstein model reduction approach for parametrized flow problems in porous media*, May 2022. arXiv:2205.02721 [cs, math].
- [4] N. BONNEEL, G. PEYRÉ, AND M. CUTURI, *Wasserstein barycentric coordinates: histogram regression using optimal transport*, ACM Trans. Graph., 35 (2016), pp. 1–10, <https://doi.org/10.1145/2897824.2925918>.
- [5] L. A. CAFFARELLI, *The regularity of mappings with a convex potential*, J. Amer. Math. Soc., 5 (1992), pp. 99–104, <https://doi.org/10.1090/S0894-0347-1992-1124980-8>.
- [6] N. CAGNIART, Y. MADAY, AND B. STAMM, *Model Order Reduction for Problems with Large Convection Effects*, in Contributions to Partial Differential Equations and Applications, B. N. Chetverushkin, W. Fitzgibbon, Y. Kuznetsov, P. Neittaanmäki, J. Periaux, and O. Pironneau, eds., vol. 47, Springer International Publishing, Cham, 2019, pp. 131–150, [https://doi.org/10.1007/978-3-319-78325-3\\_10](https://doi.org/10.1007/978-3-319-78325-3_10). Series Title: Computational Methods in Applied Sciences.
- [7] S. CHATURANTABUT AND D. C. SORENSEN, *Nonlinear Model Reduction via Discrete Empirical Interpolation*, SIAM J. Sci. Comput., 32 (2010), pp. 2737–2764, <https://doi.org/10.1137/090766498>.
- [8] M. CUTURI, *Sinkhorn Distances: Lightspeed Computation of Optimal Transport*, in Advances in Neural Information Processing Systems, vol. 26, Curran Associates, Inc., 2013.
- [9] M. CUTURI AND A. DOUCET, *Fast Computation of Wasserstein Barycenters*, in Proceedings of the 31st International Conference on Machine Learning, vol. 32 of Proceedings of Machine Learning Research, Beijing, China, 2014, PMLR, pp. 685–693.
- [10] M.-H. DO, J. FEYDY, AND O. MULA, *Approximation and Structured Prediction with Sparse Wasserstein Barycenters*, Feb. 2023. arXiv:2302.05356 [cs, math].
- [11] I. DOKMANIC, R. PARHIZKAR, J. RANIERI, AND M. VETTERLI, *Euclidean Distance Matrices: Essential theory, algorithms, and applications*, IEEE Signal Process. Mag., 32 (2015), pp. 12–30, <https://doi.org/10.1109/MSP.2015.2398954>.
- [12] V. EHRLACHER, D. LOMBARDI, O. MULA, AND F.-X. VIALARD, *Nonlinear model reduction on metric spaces. Application to one-dimensional conservative PDEs in Wasserstein spaces*, ESAIM: M2AN, 54 (2020), pp. 2159–2197, <https://doi.org/10.1051/m2an/2020013>.
- [13] J. FEYDY, *Geometric data analysis, beyond convolutions*, PhD thesis, Université Paris-Saclay, 2020.
- [14] A. GENEVAY, L. CHIZAT, F. BACH, M. CUTURI, AND G. PEYRÉ, *Sample Complexity of Sinkhorn Divergences*, in Proceedings of the Twenty-Second International Conference on Artificial Intelligence and Statistics, vol. 89 of Proceedings of Machine Learning Research, PMLR, 2019, pp. 1574–1583.
- [15] A. GENEVAY, G. PEYRÉ, AND M. CUTURI, *Learning Generative Models with Sinkhorn Divergences*, in Proceedings of the Twenty-First International Conference on Artificial Intelligence and Statistics, vol. 84 of Proceedings of Machine Learning Research, PMLR, 2018, pp. 1608–1617.

- [16] N. GIGLI, *On Hölder continuity-in-time of the optimal transport map towards measures along a curve*, Proceedings of the Edinburgh Mathematical Society, 54 (2011), pp. 401–409, <https://doi.org/10.1017/S001309150800117X>.
- [17] J.-B. HIRIART-URRUTY AND C. LEMARÉCHAL, *Fundamentals of Convex Analysis*, Springer Berlin Heidelberg, Berlin, Heidelberg, 2001, <https://doi.org/10.1007/978-3-642-56468-0>.
- [18] A. IOLLO AND D. LOMBARDI, *Advection modes by optimal mass transfer*, Phys. Rev. E, 89 (2014), p. 022923, <https://doi.org/10.1103/PhysRevE.89.022923>.
- [19] A. IOLLO AND T. TADDEI, *Mapping of coherent structures in parameterized flows by learning optimal transportation with Gaussian models*, Journal of Computational Physics, 471 (2022), p. 111671, <https://doi.org/10.1016/j.jcp.2022.111671>.
- [20] H. JANATI, M. CUTURI, AND A. GRAMFORT, *Debiased Sinkhorn barycenters*, in Proceedings of the 37th International Conference on Machine Learning, vol. 119 of PMLR, 2020.
- [21] G. LOEPER, *On the regularity of solutions of optimal transportation problems*, Acta Math., 202 (2009), pp. 241–283, <https://doi.org/10.1007/s11511-009-0037-8>.
- [22] C. LÉONARD AND MODAL-X. UNIVERSITÉ PARIS OUEST, BÂT. G, 200 AV. DE LA RÉPUBLIQUE. 92001 NANTERRE, *A survey of the Schrödinger problem and some of its connections with optimal transport*, Discrete & Continuous Dynamical Systems - A, 34 (2014), pp. 1533–1574, <https://doi.org/10.3934/dcds.2014.34.1533>.
- [23] R. J. MCCANN, *A Convexity Principle for Interacting Gases*, Advances in Mathematics, 128 (1997), pp. 153–179, <https://doi.org/10.1006/aima.1997.1634>.
- [24] C. MOOSMÜLLER AND A. CLONINGER, *Linear optimal transport embedding: provable Wasserstein classification for certain rigid transformations and perturbations*, Information and Inference: A Journal of the IMA, 12 (2023), pp. 363–389, <https://doi.org/10.1093/imaiai/iaac023>.
- [25] M. MUELLER, S. AERON, J. M. MURPHY, AND A. TASISSA, *Geometric Sparse Coding in Wasserstein Space*, Oct. 2022. arXiv:2210.12135 [cs, eess, math, stat].
- [26] Q. MÉRIGOT, A. DELALANDE, AND F. CHAZAL, *Quantitative stability of optimal transport maps and linearization of the 2-Wasserstein space*, in Proceedings of the Twenty Third International Conference on Artificial Intelligence and Statistics, vol. 108 of Proceedings of Machine Learning Research, PMLR, 2020, pp. 3186–3196.
- [27] N. J. NAIR AND M. BALAJEWICZ, *Transported snapshot model order reduction approach for parametric, steady-state fluid flows containing parameter-dependent shocks*, Int J Numer Methods Eng, 117 (2019), pp. 1234–1262, <https://doi.org/10.1002/nme.5998>.
- [28] M. OHLBERGER AND S. RAVE, *Reduced Basis Methods: Success, Limitations and Future Challenges*, in Proceedings of the Conference Algorithmy, 2016, pp. 1–12.
- [29] F. OTTO, *The geometry of dissipative evolution equations: the porous medium equation*, Communications in Partial Differential Equations, 26 (2001), pp. 101–174, <https://doi.org/10.1081/PDE-100002243>.
- [30] B. PEHERSTORFER, Z. DRMAČ, AND S. GUGERCIN, *Stability of Discrete Empirical Interpolation and Gappy Proper Orthogonal Decomposition with Randomized and Deterministic Sampling Points*, SIAM J. Sci. Comput., 42 (2020), pp. A2837–A2864, <https://doi.org/10.1137/19M1307391>.
- [31] G. PEYRÉ AND M. CUTURI, *Computational Optimal Transport*, vol. 11:5-6 of Foundations and Trends in Machine Learning, now Publishers, Delft, The Netherlands, 2019.

- [32] A.-A. POOLADIAN AND J. NILES-WEED, *Entropic estimation of optimal transport maps*, May 2022. arXiv:2109.12004 [math, stat].
- [33] A. QUARTERONI, A. MANZONI, AND F. NEGRI, *Reduced Basis Methods for Partial Differential Equations*, vol. 92 of UNITEXT, Springer International Publishing, Cham, 2016, <https://doi.org/10.1007/978-3-319-15431-2>.
- [34] A. RAMDAS, N. TRILLOS, AND M. CUTURI, *On Wasserstein Two-Sample Testing and Related Families of Nonparametric Tests*, Entropy, 19 (2017), p. 47, <https://doi.org/10.3390/e19020047>.
- [35] C. E. RASMUSSEN AND C. K. I. WILLIAMS, *Gaussian processes for machine learning*, Adaptive computation and machine learning, MIT Press, Cambridge, Mass, 2006. OCLC: ocm61285753.
- [36] P. RIGOLLET AND J. WEED, *Entropic optimal transport is maximum-likelihood deconvolution*, Comptes Rendus Mathématique, 356 (2018), pp. 1228–1235, <https://doi.org/10.1016/j.crma.2018.10.010>.
- [37] D. RIM AND K. T. MANDLI, *Displacement Interpolation Using Monotone Rearrangement*, SIAM/ASA J. Uncertainty Quantification, 6 (2018), pp. 1503–1531, <https://doi.org/10.1137/18M1168315>.
- [38] D. RIM, B. PEHERSTORFER, AND K. T. MANDLI, *Manifold Approximations via Transported Subspaces: Model Reduction for Transport-Dominated Problems*, SIAM J. Sci. Comput., 45 (2023), pp. A170–A199, <https://doi.org/10.1137/20M1316998>.
- [39] F. SANTAMBROGIO, *Optimal Transport for Applied Mathematicians*, vol. 87 of Progress in Nonlinear Differential Equations and Their Applications, Springer International Publishing, Cham, 2015, <https://doi.org/10.1007/978-3-319-20828-2>.
- [40] F. SANTAMBROGIO, { *Euclidean, Metric, and Wasserstein* } *Gradient Flows: an overview*, Sept. 2016. arXiv:1609.03890 [math].
- [41] M. A. SCHMITZ, M. HEITZ, N. BONNEEL, F. NGOLÈ, D. COEURJOLLY, M. CUTURI, G. PEYRÉ, AND J.-L. STARCK, *Wasserstein Dictionary Learning: Optimal Transport-Based Unsupervised Nonlinear Dictionary Learning*, SIAM J. Imaging Sci., 11 (2018), pp. 643–678, <https://doi.org/10.1137/17M1140431>.
- [42] J. SOLOMON, F. DE GOES, G. PEYRÉ, M. CUTURI, A. BUTSCHER, A. NGUYEN, T. DU, AND L. GUIBAS, *Convolutional wasserstein distances: efficient optimal transportation on geometric domains*, ACM Trans. Graph., 34 (2015), pp. 1–11, <https://doi.org/10.1145/2766963>.
- [43] T. TADDEI, *A Registration Method for Model Order Reduction: Data Compression and Geometry Reduction*, SIAM J. Sci. Comput., 42 (2020), pp. A997–A1027, <https://doi.org/10.1137/19M1271270>.
- [44] T. TADDEI, *An optimization-based registration approach to geometry reduction*, Nov. 2022. arXiv:2211.10275 [cs, math].
- [45] T. TADDEI AND L. ZHANG, *Space-time registration-based model reduction of parameterized one-dimensional hyperbolic PDEs*, ESAIM: M2AN, 55 (2021), pp. 99–130, <https://doi.org/10.1051/m2an/2020073>.
- [46] J. URBAS, *Mass Transfer Problems*, Tech. Report 41, Institut für angewandte Mathematik der Universität Bonn, 1998.
- [47] F. VERDUGO AND S. BADIA, *The software design of Gridap: A Finite Element package based on the Julia JIT compiler*, Computer Physics Communications, 276 (2022), p. 108341, <https://doi.org/10.1016/j.cpc.2022.108341>.

- [48] A. M. VERSHIK, *Long History of the Monge-Kantorovich Transportation Problem: (Marking the centennial of L.V. Kantorovich's birth!)*, Math Intelligencer, 35 (2013), pp. 1–9, <https://doi.org/10.1007/s00283-013-9380-x>.
- [49] C. VILLANI, *Topics in optimal transportation*, no. 58 in Graduate studies in mathematics, American Mathematical Society, Providence, Rhode Island, reprinted with corrections ed., 2016.
- [50] W. WANG, D. SLEPČEV, S. BASU, J. A. OZOLEK, AND G. K. ROHDE, *A Linear Optimal Transportation Framework for Quantifying and Visualizing Variations in Sets of Images*, Int J Comput Vis, 101 (2013), pp. 254–269, <https://doi.org/10.1007/s11263-012-0566-z>.
- [51] G. WELPER, *Interpolation of Functions with Parameter Dependent Jumps by Transformed Snapshots*, SIAM J. Sci. Comput., 39 (2017), pp. A1225–A1250, <https://doi.org/10.1137/16M1059904>.
- [52] M. WERENSKI, R. JIANG, A. TASISSA, S. AERON, AND J. M. MURPHY, *Measure Estimation in the Barycentric Coding Model*, in Proceedings of the 39th International Conference on Machine Learning, vol. 162 of Proceedings of Machine Learning Research, Baltimore, Maryland, USA, 2022, PMLR, pp. 23781–23803.
- [53] M. YANO AND A. T. PATERA, *An LP empirical quadrature procedure for reduced basis treatment of parametrized nonlinear PDEs*, Computer Methods in Applied Mechanics and Engineering, 344 (2019), pp. 1104–1123, <https://doi.org/10.1016/j.cma.2018.02.028>.